Supporting Information

Section Introduction

Figure S1: Schematics of the flow dynamics in a far field approximation (not to scale). Blue color marks the planar interface (dashed) and the perturbed interface (solid).

Fig. S1

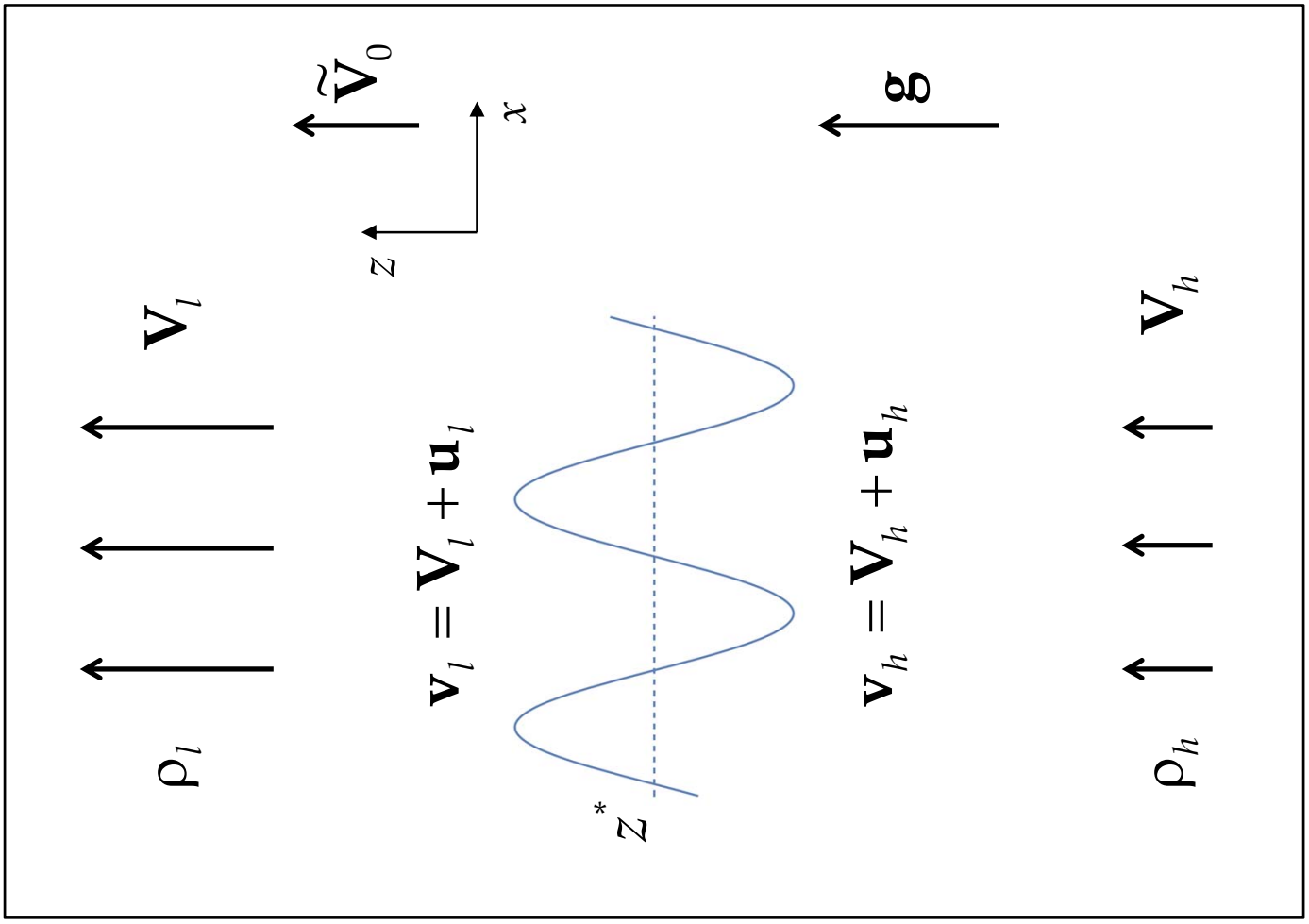
ρ_l
$\mathbf{V}_l$
$\mathbf{v}_l = \mathbf{V}_l + \mathbf{u}_l$
$\tilde{\mathbf{V}}_0$
x
z
z^*
$\mathbf{g}$
$\mathbf{v}_h = \mathbf{V}_h + \mathbf{u}_h$
ρ_h
$\mathbf{V}_h$

Section Methods

Sub-section Governing equation

The governing equations in the bulk

$$\partial\rho/\partial t+\partial\rho v_i/\partial x_i=0\,,\ \ \partial\rho v_i/\partial t+\sum_{j=1}^{3}\partial\rho v_i v_j/\partial x_i+\partial P/\partial x_i=0\,,\ \ \partial E/\partial t+\partial(E+P)v_i/\partial x_i=0 \qquad \text{(SI-1a)}$$

and the boundary conditions at the interface

$$\left[\tilde{\mathbf{j}}\cdot\mathbf{n}\right]=0\,,\ \left[\left(P+\left(\tilde{\mathbf{j}}\cdot\mathbf{n}\right)^2/\rho\right)\mathbf{n}\right]=0\,,\ \left[\left(\tilde{\mathbf{j}}\cdot\mathbf{n}\right)\left(\left(\tilde{\mathbf{j}}\cdot\boldsymbol{\tau}\right)/\rho\right)\boldsymbol{\tau}\right]=0\,,\ \left[\left(\tilde{\mathbf{j}}\cdot\mathbf{n}\right)\left(W+\tilde{\mathbf{j}}^2/2\rho^2\right)\right]=0 \qquad \text{(SI-1b)}$$

are applicable for both compressible and incompressible fluids. Boundary conditions Eqs.(SI-1b) are derived by representing the flow fields as $(\rho,\mathbf{v},P,E)=(\rho,\mathbf{v},P,E)_h H(\theta)+(\rho,\mathbf{v},P,E)_l H(-\theta)$ in Eqs.(SI-1a), where $H(\theta)$ is the Heaviside step-function, and $\partial H/\partial\theta=\delta(\theta)$ with $\delta(\theta)$ being the Dirac delta-function.

We use the physics definition of W and e [5,6]. Particularly, the specific internal energy e refers to energy per unit mass contained within a system, excluding the kinetic energy and the potential energy of the system as a whole. The initial conditions are the initial flow fields at the interface. They define the characteristic scales of length $1/k$ and time $1/kV_h$ for the dynamics [5,6].

Sub-section Linearized dynamics

The boundary conditions (SI-1b) can be linearized. To the leading order and the first order

$$\left[J_n\right]=0,\ \left[\left(P_0+J_n^2/\rho\right)\mathbf{n}_0\right]=0,\ \left[J_n\left((\mathbf{J}\cdot\boldsymbol{\tau}_0)/\rho\right)\boldsymbol{\tau}_0\right]=0,\ \left[J_n\left(W_0+\mathbf{J}^2/2\rho^2\right)\right]=0, \tag{SI-1c}$$

$$\left[j_n\right]=0,\ \left[\left(p+2J_nj_n/\rho\right)\mathbf{n}_0\right]=0,\ \left[J_n\left(\mathbf{J}\cdot\boldsymbol{\tau}_1+\mathbf{j}\cdot\boldsymbol{\tau}_0\right)/\rho\right]=0,\ \left[J_n\left(w+(\mathbf{J}\cdot\mathbf{j})/\rho^2\right)\right]=0, \tag{SI-1d}$$

Expansions Eqs.(SI-1c,d) are applicable for both compressible and incompressible dynamics. In the incompressible case, Eqs.(SI-1c,d) can be further simplified. Particularly, for ideal gases, the speed of sound is $c=\sqrt{\gamma P/\rho}$, where γ is the fluid's adiabatic index. In the incompressible case the speed of sound is the largest velocity scale, with $\left(c/V_{h(l)}\right)\to\infty$, and values approach $\left(P_0+J_n^2/\rho\right)_{h(l)}\to\left(P_0\right)_{h(l)}$ and $\left(W_0+\mathbf{J}^2/2\rho^2\right)_{h(l)}\to\left(W_0\right)_{h(l)}$ transforming Eqs.(SI-1c) to

$$\left[J_n\right]=0,\ \left[P_0\,\mathbf{n}_0\right]=0,\ \left[J_n\left((\mathbf{J}\cdot\boldsymbol{\tau}_0)/\rho\right)\boldsymbol{\tau}_0\right]=0,\ \left[J_nW_0\right]=0, \tag{SI-1e}$$

where the specific enthalpy is $\left(W_0\right)_{h(l)}=\left(\overline{W}_0+c_PT\right)_{h(l)}$. Here $\left(c_P\right)_{h(l)}$ is the specific heat at constant pressure, $\left(T\right)_{h(l)}$ is temperature, and the values $\left(\overline{W}_0\right)_{h(l)}$ have a constant jump at the interface $\left[\overline{W}_0\right]=\overline{Q}$, where $\overline{Q}$ is the heat release per unit mass. In reactive fluids, the value $\overline{Q}$ is considered as the specific heat release of a chemical reaction at the absolute zero temperature. In Eqs.(SI-1d) the incompressible condition leads to enthalpy perturbations $w_{h(l)}=p_{h(l)}/\rho_{h(l)}$.

This derivation is similar to that in Landau-Lifshitz Theory Course V6 Hydrodynamics #128, Eqs.(128.3, 128.4) with appropriate change of variables.

Note the difference in definitions of enthalpy W in physics sense and $\overline{W}$ in engineering sense.

Sub-section Fundamental solutions

a. Solutions structure

The governing equations are reduced to a linear system $\mathrm{M}\,\mathbf{r}=0$, where $\mathbf{r}=\left(\Phi_h,\Phi_l,V_h z^*,\Psi_l\right)^{\mathrm{T}}$ is a vector and M is a 4x4 matrix. The matrix M is defined by the boundary conditions at the interface. Its elements are functions of ω, R and G. We find eigenvalues ω_i by using condition $det\,\mathrm{M}\left(\omega_i,R,G\right)=0$ and identify the associated eigenvectors $\mathbf{e}_i$ by reducing matrix $\mathrm{M}=\mathrm{M}\left(\omega_i,R,G\right)$ to row-echelon form. For a non-degenerate 4×4 matrix with rank 4, the expected number of eigenvalues ω_i and associated eigenvectors $\mathbf{e}_i$ is 4, with $i=1...4$, corresponding to 4 degrees of freedom and 4 independent variables obeying 4 equations. The solution $\mathbf{r}$ is a linear combination of fundamental solutions $\mathbf{r}_i=\mathbf{r}_i\left(\omega_i,\mathbf{e}_i\right)$ as $\mathbf{r}=\sum_i C_i\mathbf{r}_i$, where C_i are the integration constants set, e.g., by the initial conditions.

Note that the linear system $\mathrm{M}\,\mathbf{r}=0$ with $\mathrm{M}=\mathrm{M}(\omega,R,G)$ results from a linear system $\mathrm{P}\dot{\mathbf{r}}=\mathrm{S}\mathbf{r}$ where P,S are 4×4 matrixes with $\mathrm{P}=\mathrm{P}(\mathrm{R},\mathrm{G}),\mathrm{S}=\mathrm{S}(\mathrm{R},\mathrm{G})$, under assumption that vector $\mathbf{r}$ varies in time as $\mathbf{r}\sim e^{\omega t}$. This leads to $\mathrm{M}=(\mathrm{S}-\omega\mathrm{P})$. In a non-degenerate case, the inverse P^{-1} exists, and the system $\mathrm{P}\dot{\mathbf{r}}=\mathrm{S}\mathbf{r}$ can be reduced to a standard form $\dot{\mathbf{r}}=\mathrm{P}^{-1}\mathrm{S}\mathbf{r}$. The eigenvalues ω_i of the dynamics can then be found from the conditions $det\left(\mathrm{P}^{-1}\mathrm{S}-\omega\mathrm{I}\right)=0$, where $\omega=\{\omega_i\}$, I is the unit matrix, and index i marks the independent degrees of freedom. Equations $det\left(\mathrm{P}^{-1}\mathrm{S}-\omega\mathrm{I}\right)=0$ and $det\,\mathrm{M}(\omega,R,G)=0$ have the same eigenvalues ω_i because linear combination of differential equations preserves the dynamical properties.

Our approach for the boundary value problem and initial value problem systematically applies the standard rigorous methods of applied mathematics and theoretical physics. Specifically, we consider the conservation laws of mass, momentum and energy in the inertial reference frame; derive the boundary conditions; linearize the dynamics; expand the perturbations of the flow fields by using scalar and vector potentials; derive the linear system; find the fundamental solutions for the linear system; employ the eigenvalues and eigenvectors of the fundamental solutions; study the formal, qualitative and quantitative properties of the dynamics.

b. Derivation details

In accordance with PNAS Policy on Materials and Data Availability, the authors report that the algebraic calculations of matrices, eigenvalues, and eigenvectors were done using standard linear algebra procedures, as described in the text. These can be done manually and/or with standard computer algebra software such as Wolfram Mathematica. The plots were generated in Wolfram Mathematica by assigning numerical values to variables, as described in the text.

Section Results – Inertial dynamics

Sub-section Conservative dynamics

a. Fundamental solutions

For inertial conservative dynamics, with $\mathrm{M}\,\mathbf{r} = 0$ and $\mathbf{r} = \left(\Phi_h, \Phi_l, V_h z^*, \Psi_l\right)$, matrix $\mathrm{M} = M$ is

$$M = \begin{pmatrix} -R & -1 & -\omega + R\omega & i \\ 1 & -1 & 1-R & i\omega/R \\ R - R\omega & R + \omega & 0 & -2iR \\ \omega & -\omega & \omega - R\omega & iR \end{pmatrix}.$$

Fundamental solution $\mathbf{r}_1(\omega_1, \mathbf{e}_1)$ has the eigenvalue ω_1 and eigenvector $\mathbf{e}_1$:

$$\omega_1 = i\sqrt{R}\ , \quad \mathbf{e}_1 = \begin{pmatrix} i\dfrac{-1+R}{i+\sqrt{R}} \\ -\dfrac{-1+R}{i+\sqrt{R}}\sqrt{R} \\ 1 \\ 0 \end{pmatrix}.$$

Fundamental solution $\mathbf{r}_2(\omega_2, \mathbf{e}_2)$ has the eigenvalue ω_2 and eigenvector $\mathbf{e}_2$:

$$\omega_2 = -i\sqrt{R}\ , \quad \mathbf{e}_2 = \begin{pmatrix} -i\dfrac{-1+R}{-i+\sqrt{R}} \\ -\dfrac{-1+R}{-i+\sqrt{R}}\sqrt{R} \\ 1 \\ 0 \end{pmatrix}.$$

Fundamental solution $\mathbf{r}_3(\omega_3, \mathbf{e}_3)$ has the eigenvalue ω_3 and eigenvector $\mathbf{e}_3$:

$$\omega_3 = R\ , \quad \mathbf{e}_3 = \begin{pmatrix} 0 \\ i \\ 0 \\ 1 \end{pmatrix}.$$

Fundamental solution $\mathbf{r}_4(\omega_4, \mathbf{e}_4)$ has the eigenvalue ω_4 and eigenvector $\mathbf{e}_4$:

$$\omega_4 = -R\ , \quad \mathbf{e}_4 = \begin{pmatrix} \dfrac{2i}{1+R} \\ -\dfrac{i(-1+R)}{1+R} \\ 0 \\ 1 \end{pmatrix}.$$

b. Figure captions and Figures

Figure S2: Flow fields' structure for the inertial conservative dynamics, fundamental solution $\mathbf{r}_{CD}\left(\omega_{CD},\mathbf{e}_{CD}\right)$ with $\mathbf{r}_{CD}=\left(\mathbf{r}_1+\mathbf{r}_2\right)/2$. Plots of the perturbed velocity vector fields $\mathbf{u}_{h(l)}$, the perturbed velocity streamlines $\mathbf{s}_{h(l)}$, the contour plot of the perturbed pressure $p_{h(l)}$, and the interface perturbation z^* in the (x,z) plane. For this solution, the vortical field is $\nabla\times\mathbf{\Psi}_l=0,\nabla\times\mathbf{u}_l=0$. Density ratio is $R=5$, time $t=\pi/2$, $[t]=1/kV_h$. Values are $|p_l|_{\max(\min)}/|p_h|_{\max(\min)}=1$. Red (blue) marks positive (negative) values in contour plots. Real parts of fields and functions are shown.

Figure S3: Flow fields' structure for inertial conservative dynamics, fundamental solution $\mathbf{r}_1\left(\omega_1,\mathbf{e}_1\right)$. Plots of the perturbed velocity vector fields $\mathbf{u}_{h(l)}$, the perturbed velocity streamlines $\mathbf{s}_{h(l)}$, and the contour plot of the perturbed pressure $p_{h(l)}$, and the interface perturbation z^* in the (x,z) plane. For this solution, the vortical field is $\nabla\times\mathbf{\Psi}_l=0,\nabla\times\mathbf{u}_l=0$. Density ratio is $R=5$, time $t=\pi/2$, $[t]=1/kV_h$. Values are $|p_l|_{\max(\min)}/|p_h|_{\max(\min)}=1$. Red (blue) marks positive (negative) values in contour plots. Real parts of fields and functions are shown.

Figure S4: Flow fields' structure for inertial conservative dynamics, fundamental solution $\mathbf{r}_3\left(\omega_3,\mathbf{e}_3\right)$. (a) Plots of the perturbed velocity vector fields $\mathbf{u}_{h(l)}$, the perturbed velocity streamlines $\mathbf{s}_{h(l)}$, and the contour plot of the perturbed pressure $p_{h(l)}$, and the interface perturbation z^* in (x,z) plane. (b) Plots of the perturbed velocity vortical filed $\nabla\times\mathbf{\Psi}_l$ and the contour plot of vorticity $\nabla\times\mathbf{u}_l$ in (x,z) plane. Density ratio is $R=5$, time $t=\pi/2$, $[t]=1/kV_h$. Values are $|p_l|_{\max(\min)}/|p_h|_{\max(\min)}=1$. Red (blue) marks positive (negative) values in contour plots. Real parts of fields and functions are shown.

Figure S5: Flow fields' structure for inertial conservative dynamics, fundamental solution $\mathbf{r}_4\left(\omega_4,\mathbf{e}_4\right)$. (a) Plots of the perturbed velocity vector fields $\mathbf{u}_{h(l)}$, the perturbed velocity streamlines $\mathbf{s}_{h(l)}$, and the contour plot of the perturbed pressure $p_{h(l)}$, and the interface perturbation z^* in (x,z) plane. (b) Plots of the perturbed velocity vortical field $\nabla\times\mathbf{\Psi}_l$ and the contour plot of vorticity $\nabla\times\mathbf{u}_l$ in (x,z) plane. Density ratio $R=5$, time $t=\pi/2$, $[t]=1/kV_h$. The values are $|p_l|_{\max(\min)}/|p_h|_{\max(\min)}=1$. Red (blue) marks positive (negative) values in contour plots. Real parts of fields and functions are shown.

Fig. S2

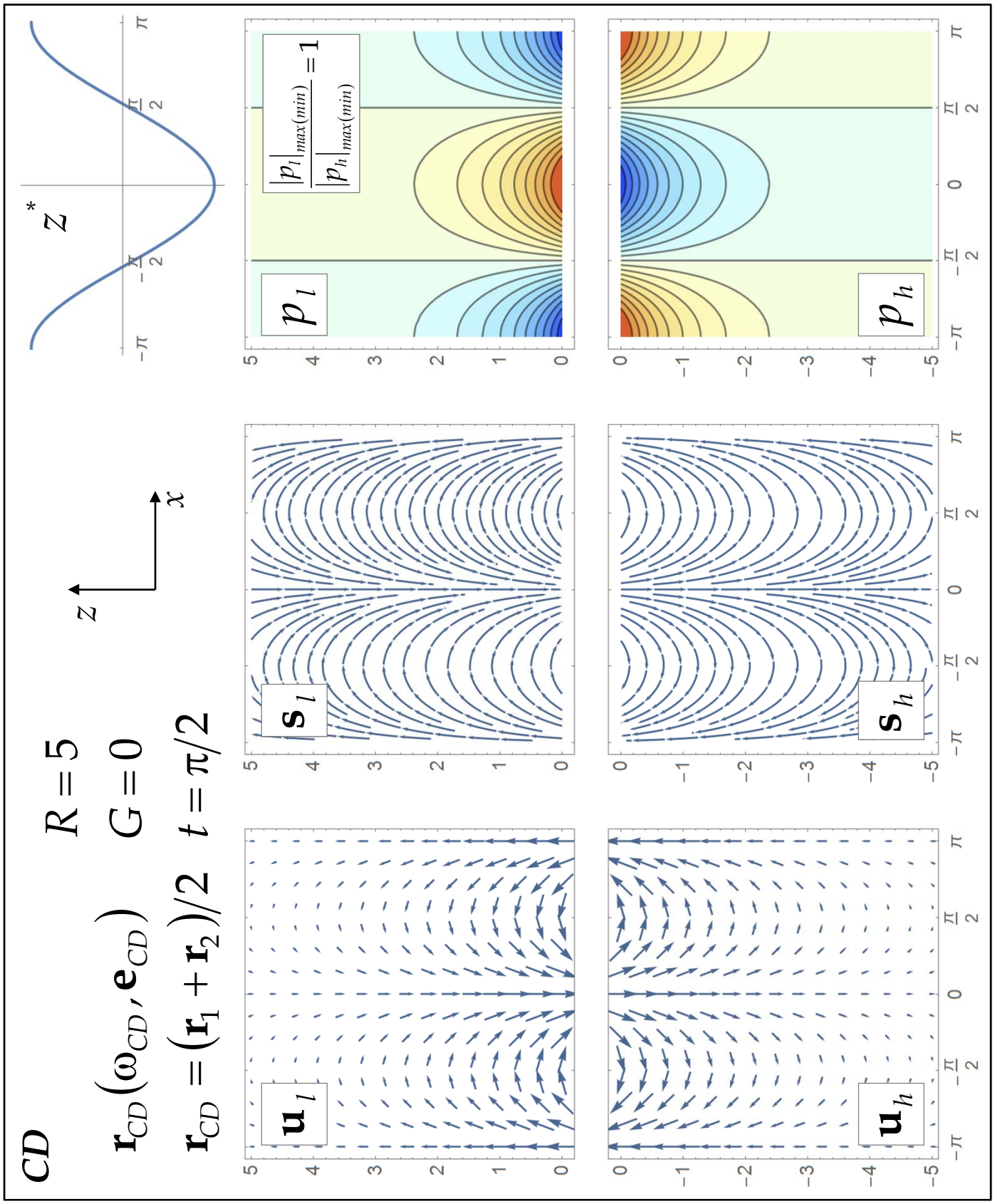
CD
$R = 5$
$G = 0$
$\mathbf{r}_{CD}\left(\omega_{CD}, \mathbf{e}_{CD}\right)$
$\mathbf{r}_{CD} = \left(\mathbf{r}_1 + \mathbf{r}_2\right)/2$ $t = \pi/2$
z
x
z^*
$\mathbf{u}_l$
$\mathbf{s}_l$
p_l
$\frac{|p_l|_{max(min)}}{|p_h|_{max(min)}} = 1$
$\mathbf{u}_h$
$\mathbf{s}_h$
p_h

Fig. S3

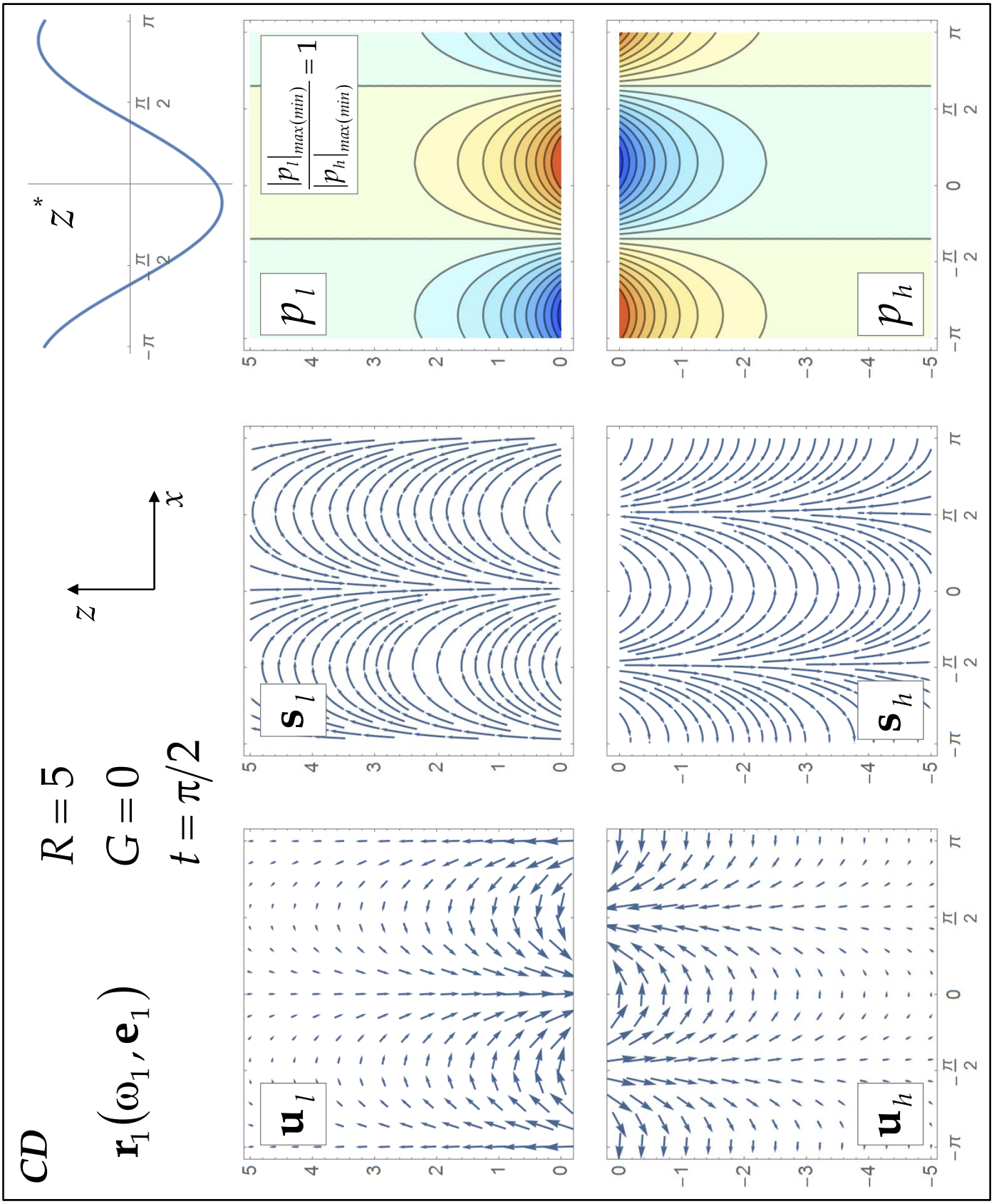
CD
$\mathbf{r}_1(\omega_1, \mathbf{e}_1)$
$R = 5$
$G = 0$
$t = \pi/2$
z
x
z^*
p_l
p_h
$\mathbf{s}_l$
$\mathbf{s}_h$
$\mathbf{u}_l$
$\mathbf{u}_h$
$\frac{|p_l|_{max(min)}}{|p_h|_{max(min)}} = 1$

Fig. S4a

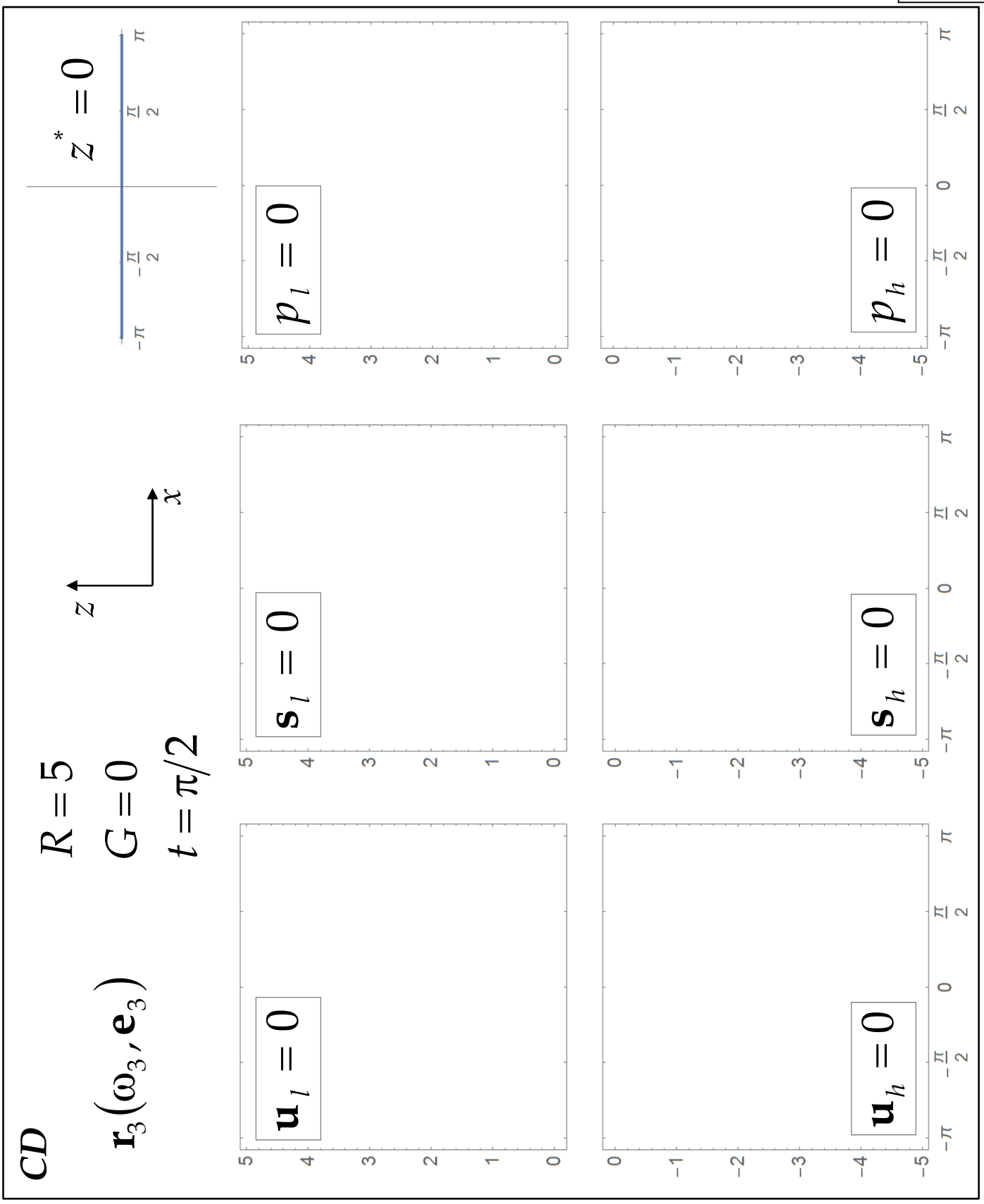
CD
$\mathbf{r}_3(\omega_3, \mathbf{e}_3)$
$R = 5$
$G = 0$
$t = \pi/2$
z
x
$z^* = 0$
$\mathbf{u}_l = 0$
$\mathbf{s}_l = 0$
$p_l = 0$
$\mathbf{u}_h = 0$
$\mathbf{s}_h = 0$
$p_h = 0$

Fig. S4b

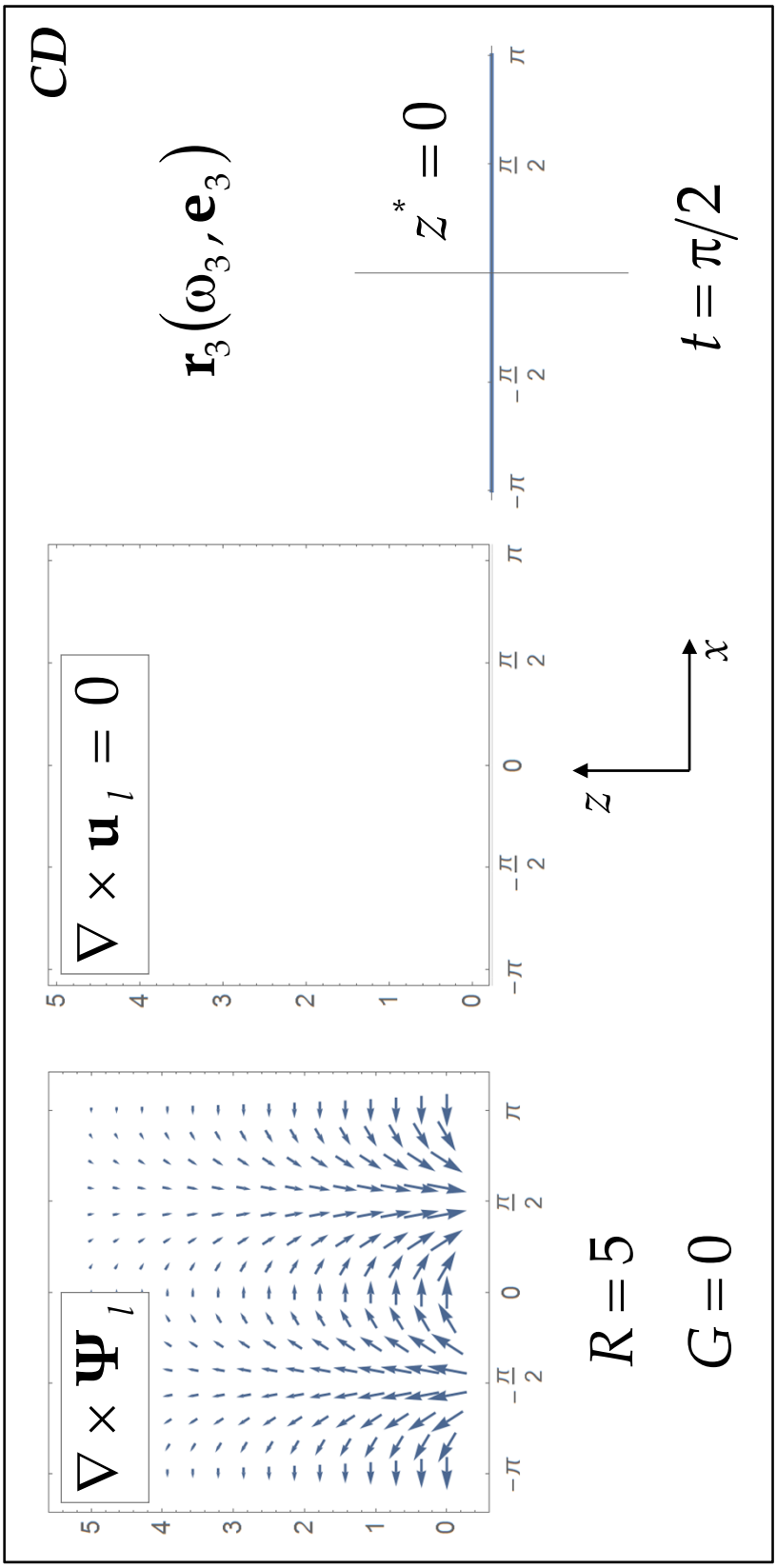
CD
$\mathbf{r}_3(\omega_3, \mathbf{e}_3)$
$z^* = 0$
$t = \pi/2$
$\nabla \times \mathbf{u}_l = 0$
$\nabla \times \Psi_l$
$R = 5$
$G = 0$
z
x

Fig. S5a

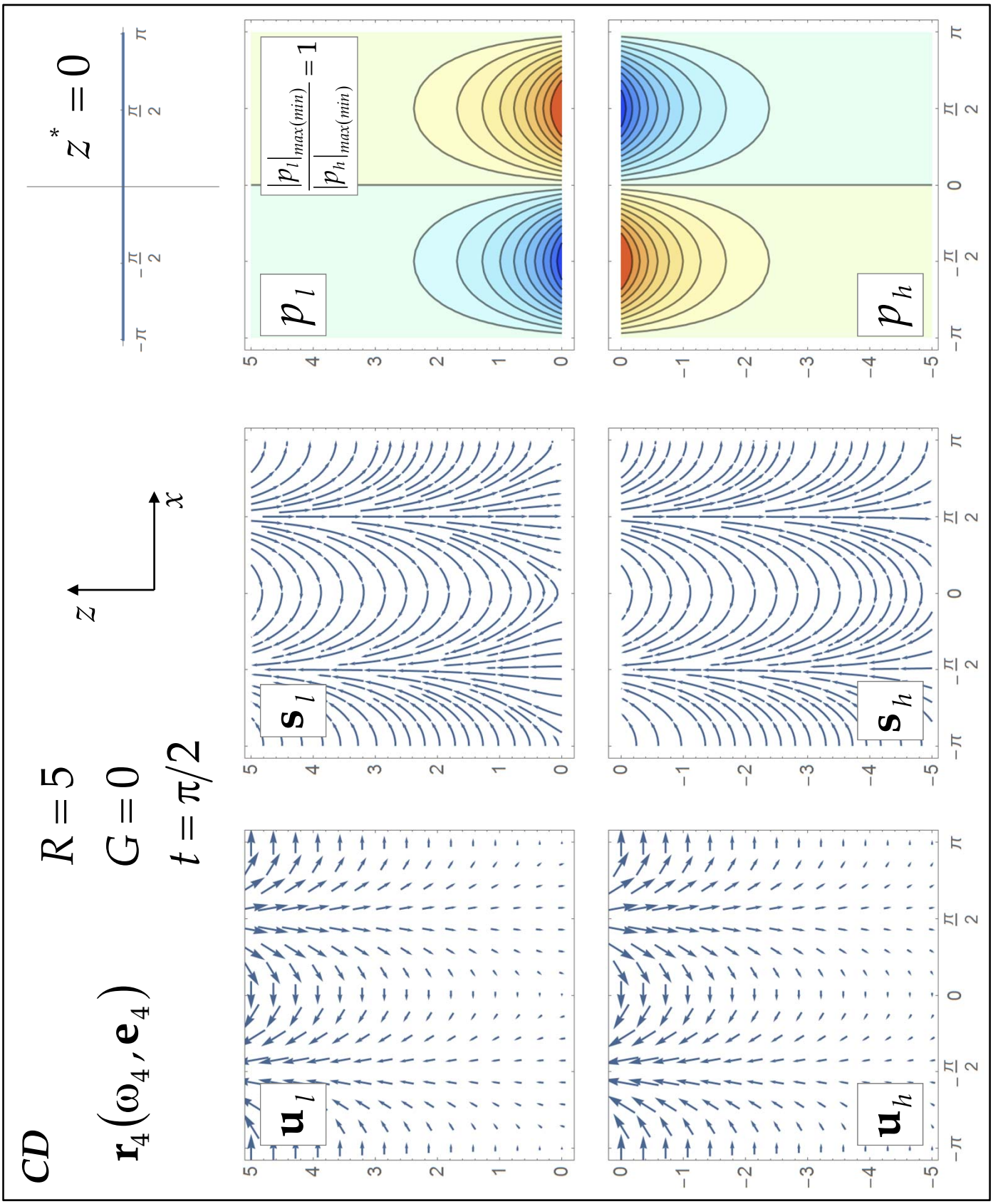
CD
$\mathbf{r}_4(\omega_4, \mathbf{e}_4)$
$R = 5$
$G = 0$
$t = \pi/2$
z
x
$z^* = 0$
$\mathbf{u}_l$
$\mathbf{s}_l$
p_l
$\frac{|p_l|_{max(min)}}{|p_h|_{max(min)}} = 1$
$\mathbf{u}_h$
$\mathbf{s}_h$
p_h

Fig. S5b

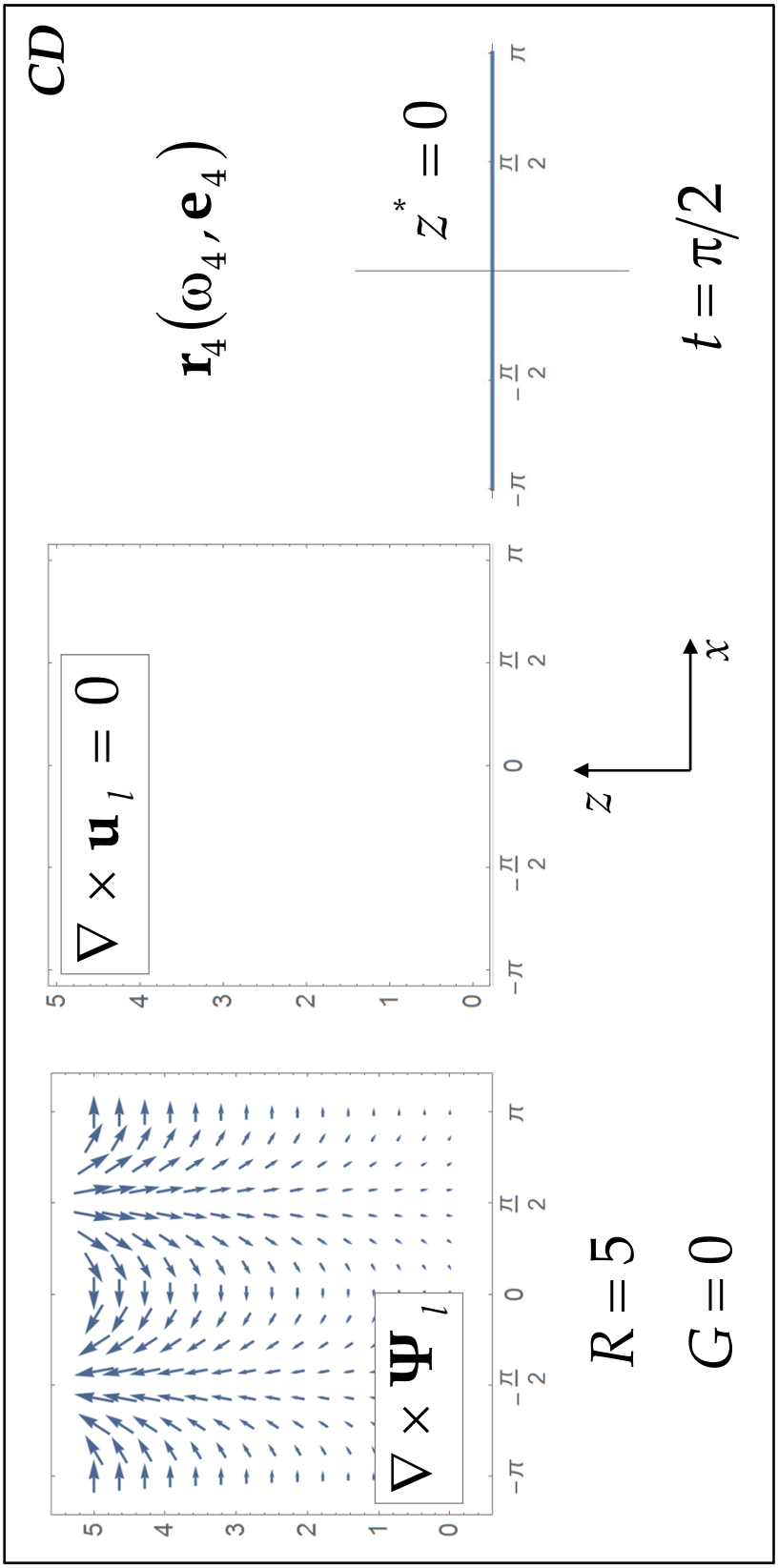
CD
$\mathbf{r}_4(\omega_4, \mathbf{e}_4)$
$z^* = 0$
$t = \pi/2$
$\nabla \times \mathbf{u}_l = 0$
$\nabla \times \Psi_l$
$R = 5$
$G = 0$
z
x

c. Non-degeneracy of conservative dynamics

For matrix $\mathrm{M} = M$ for conservative dynamics, the associated matrices $\mathrm{S} = S_M$ and $\mathrm{P} = P_M$ are

$$S_M = \begin{pmatrix} -R & -1 & 0 & i \\ 1 & -1 & 1-R & 0 \\ R & R & 0 & -2iR \\ 0 & 0 & 0 & iR \end{pmatrix}, \quad P_M = \begin{pmatrix} 0 & 0 & 1-R & 0 \\ 0 & 0 & 0 & -i/R \\ R & -1 & 0 & 0 \\ -1 & 1 & -1+R & 0 \end{pmatrix}.$$

Determinant is $det\left(\mathrm{P}^{-1}\mathrm{S} - \omega\mathrm{I}\right) = \left(\omega - R\right)\left(\omega + R\right)\left(\omega^2 + R\right)$.

The solutions of equations $det\left(\mathrm{P}^{-1}\mathrm{S} - \omega\mathrm{I}\right) = 0$ and $det\, M\left(\omega, R\right) = 0$ yield the same eigenvalues: $\omega_{1(2)} = \pm i\sqrt{R}$, $\omega_3 = R$, $\omega_4 = -R$.

For conservative dynamics, there are 4 eigenvalues, 4 fundamental solutions, and 4 degrees of freedom. The conservative dynamics is non-degenerate.

Sub-section Classic Landau's dynamics

a. Fundamental solutions

For classic Landau's dynamics, with $\mathrm{M}\,\mathbf{r} = 0$ and $\mathbf{r} = \left(\Phi_h, \Phi_l, V_h z^*, \Psi_l\right)$, the matrix $\mathrm{M} = L$ is

$$L = \begin{pmatrix} -R & -1 & -\omega + R\omega & i \\ 1 & -1 & 1-R & i\omega/R \\ R - R\omega & R+\omega & 0 & -2iR \\ -1 & -1 & 0 & i \end{pmatrix}.$$

Fundamental solution $\mathbf{r}_1(\omega_1, \mathbf{e}_1)$ has the eigenvalue ω_1 and eigenvector $\mathbf{e}_1$:

$$\omega_1 = \frac{-R + \sqrt{-R + R^2 + R^3}}{1+R}, \quad \mathbf{e}_1 = \begin{pmatrix} -i\dfrac{\left(1+\sqrt{R\left(-1+R+R^2\right)}\right)}{(-1+R)(1+R)} \\ i\dfrac{\left(R^2+\sqrt{R\left(-1+R+R^2\right)}\right)}{(-1+R)(1+R)} \\ -i\dfrac{\left(R^2+\sqrt{R\left(-1+R+R^2\right)}\right)}{(-1+R)^2 R} \\ 1 \end{pmatrix}.$$

Fundamental solution $\mathbf{r}_2(\omega_2, \mathbf{e}_2)$ has the eigenvalue ω_2 and eigenvector $\mathbf{e}_2$:

$$\omega_2 = \frac{-R - \sqrt{-R + R^2 + R^3}}{1+R}, \quad \mathbf{e}_2 = \begin{pmatrix} i\dfrac{\left(-1+\sqrt{R\left(-1+R+R^2\right)}\right)}{(-1+R)(1+R)} \\ i\dfrac{\left(R^2-\sqrt{R\left(-1+R+R^2\right)}\right)}{(-1+R)(1+R)} \\ -i\dfrac{\left(R^2-\sqrt{R\left(-1+R+R^2\right)}\right)}{(-1+R)^2 R} \\ 1 \end{pmatrix}.$$

Fundamental solution $\mathbf{r}_3(\omega_3, \mathbf{e}_3)$ has the eigenvalue ω_3 and eigenvector $\mathbf{e}_3$:

$$\omega_3 = R\ , \quad \mathbf{e}_3 = \begin{pmatrix} 0 \\ i \\ 0 \\ 1 \end{pmatrix}.$$

b. Figure captions and Figures

Figure S6: Flow fields' structure for the classic Landau's dynamics, fundamental solution $\mathbf{r}_{LD}\left(\omega_{LD}, \mathbf{e}_{LD}\right)$ with $\mathbf{r}_{LD} = \mathbf{r}_1$. (a) Plots of the perturbed velocity vector fields $\mathbf{u}_{h(l)}$, the perturbed velocity streamlines $\mathbf{s}_{h(l)}$, the contour plot of the perturbed pressure $p_{h(l)}$, and the interface perturbation z^* in (x,z) plane. (b) Plots of the perturbed velocity vortical component $\nabla \times \mathbf{\Psi}_l$, the contour plot of vorticity $\nabla \times \mathbf{u}_l$, and the interface perturbation z^* in the (x,z) plane. Density ratio is $R=5$, time is $t = \pi/2$, $[t] = 1/kV_h$. The values are $|p_l|_{\max(\min)} / |p_h|_{\max(\min)} = 1$. Red (blue) marks positive (negative) values in contour plots. Real parts of fields and functions are shown.

Figure S7: Flow fields' structure for the classic Landau dynamics, fundamental solution $\mathbf{r}_2\left(\omega_2, \mathbf{e}_2\right)$. (a) Plots of the perturbed velocity vector fields $\mathbf{u}_{h(l)}$, the perturbed velocity streamlines $\mathbf{s}_{h(l)}$, the contour plot of the perturbed pressure $p_{h(l)}$, and the interface perturbation z^* in (x,z) plane. The values are $|p_l|_{\max(\min)} / |p_h|_{\max(\min)} = 1$. (b) Plots of the perturbed velocity vortical component $\nabla \times \mathbf{\Psi}_l$ and the contour plot of vorticity $\nabla \times \mathbf{u}_l$ and the interface perturbation z^* in the (x,z) plane. Density ratio is $R=5$, time is $t = \pi/2$, $[t] = 1/kV_h$. Red (blue) marks positive (negative) values in contour plots. Real parts of fields and functions are shown.

Fig. S6a

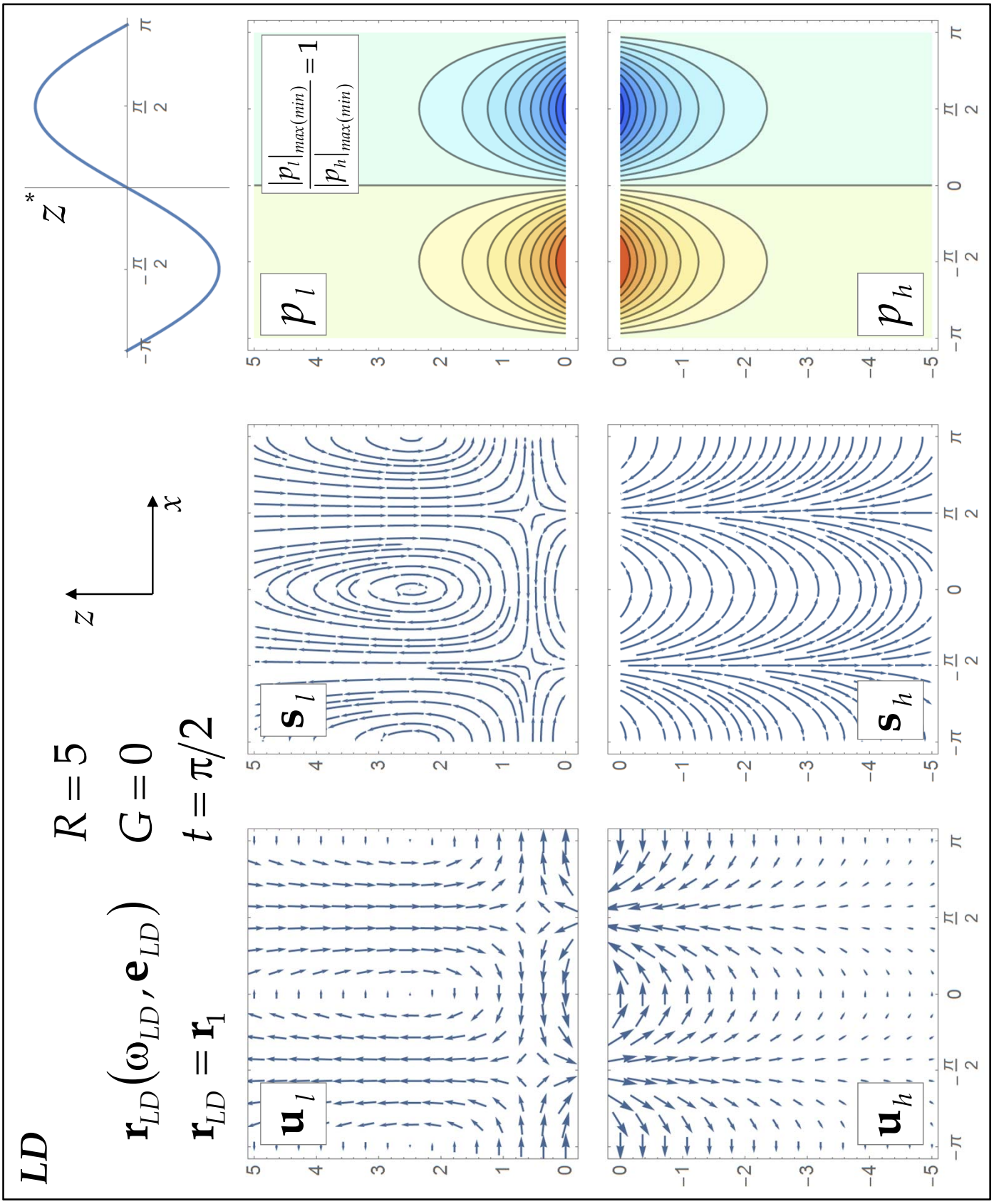
LD
$\mathbf{r}_{LD}\left(\omega_{LD}, \mathbf{e}_{LD}\right)$
$R = 5$
$G = 0$
$\mathbf{r}_{LD} = \mathbf{r}_1$
$t = \pi/2$
z
x
Z^*
$\mathbf{u}_l$
$\mathbf{s}_l$
p_l
$\frac{|p_l|_{max(min)}}{|p_h|_{max(min)}} = 1$
$\mathbf{u}_h$
$\mathbf{s}_h$
p_h

Fig. 6b

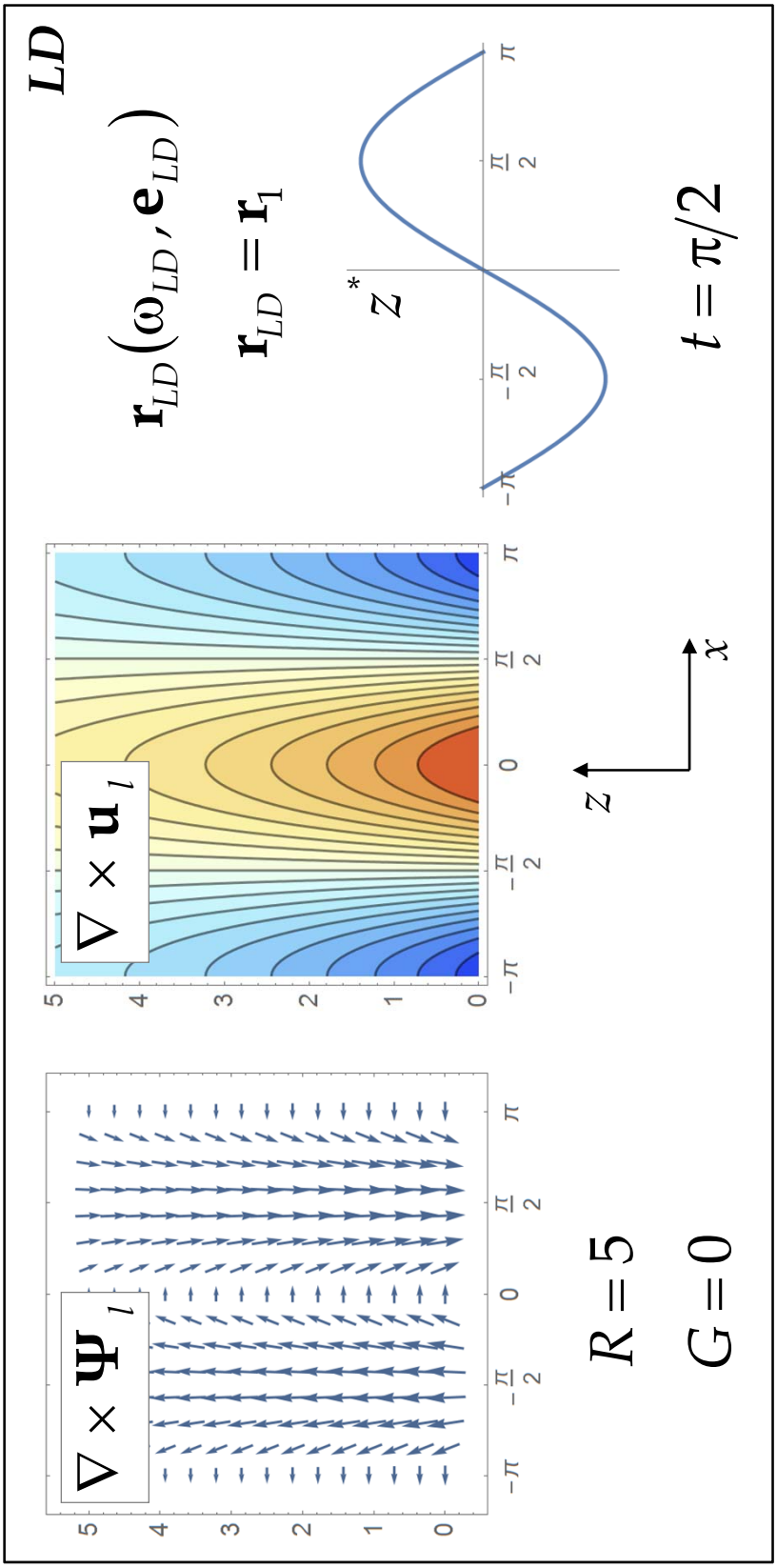
LD
$\mathbf{r}_{LD}(\omega_{LD}, \mathbf{e}_{LD})$
$\mathbf{r}_{LD} = \mathbf{r}_1$
Z^*
$t = \pi/2$
$\nabla \times \mathbf{u}_l$
$\nabla \times \boldsymbol{\Psi}_l$
z
x
$R = 5$
$G = 0$

Fig. S7a

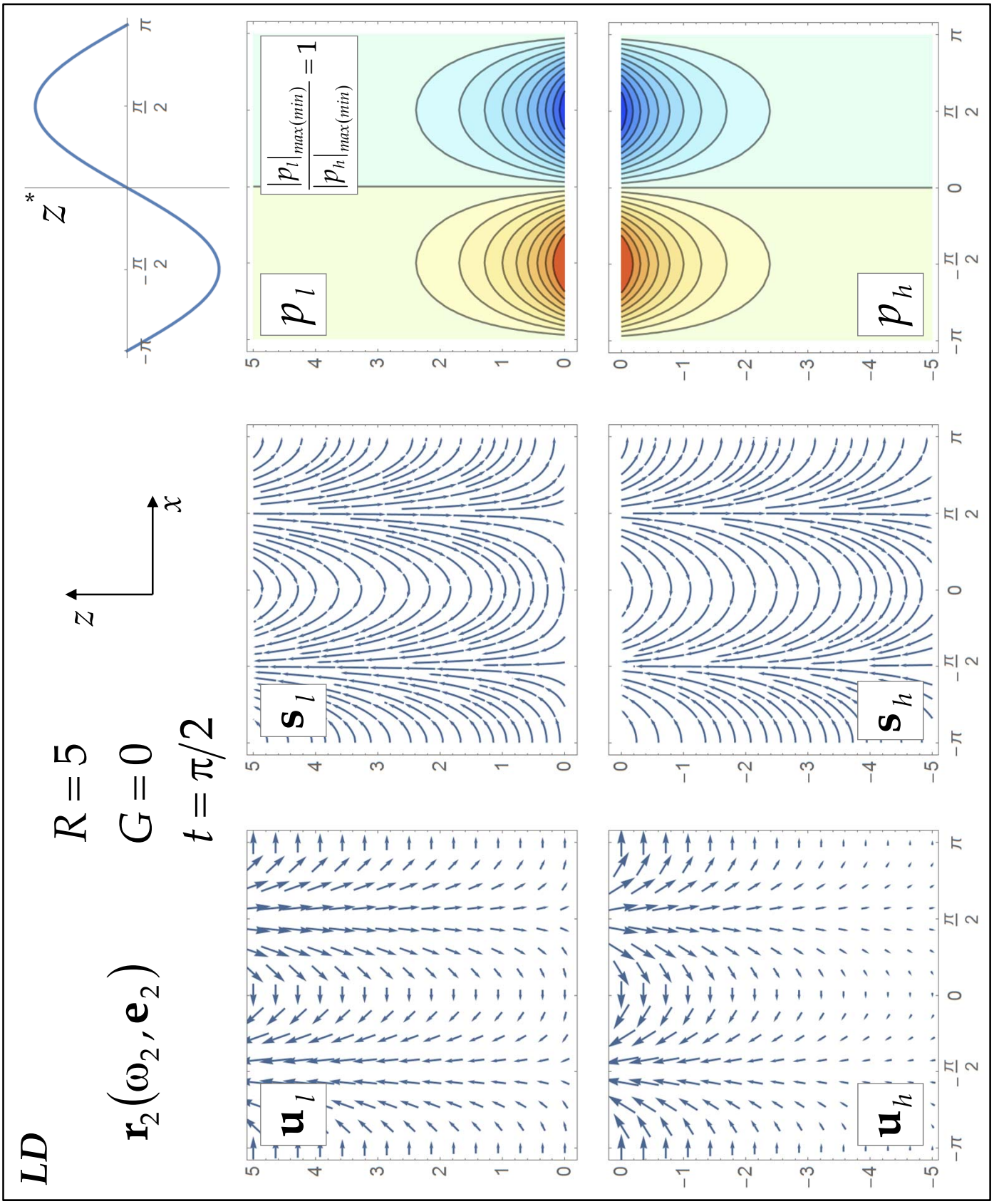
LD
$\mathbf{r}_2(\omega_2, \mathbf{e}_2)$
$R = 5$
$G = 0$
$t = \pi/2$
z
x
Z^*
$\mathbf{u}_l$
$\mathbf{s}_l$
p_l
$\frac{|p_l|_{max(min)}}{|p_h|_{max(min)}} = 1$
$\mathbf{u}_h$
$\mathbf{s}_h$
p_h

Fig. S7b

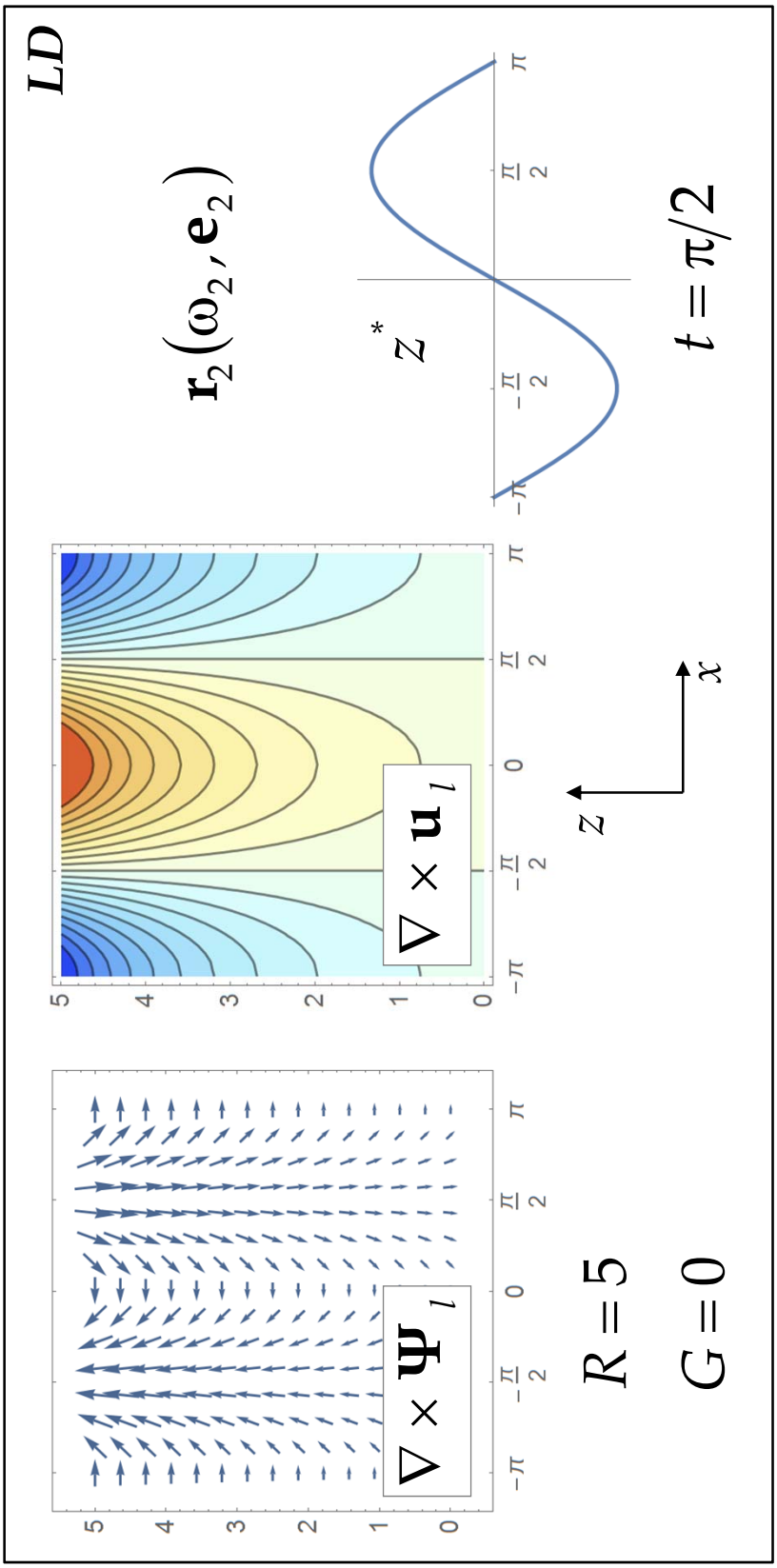
LD
$\mathbf{r}_2(\omega_2, \mathbf{e}_2)$
Z^*
$t = \pi/2$
$\nabla \times \mathbf{u}_1$
$\nabla \times \boldsymbol{\Psi}_1$
z
x
$R = 5$
$G = 0$

c. Degenerate character of Landau's dynamics

The classic Landau dynamics has smaller than expected number of fundamental solutions. This paradox can be understood from the following consideration. The linear system $L\mathbf{r} = 0$ results from a linear system $P_L\dot{\mathbf{r}} = S_L\mathbf{r}$ as $L = (S_L - \omega P_L)$, assuming $\mathbf{r} \sim e^{\omega t}$. The associated matrices S_L and P_L are

$$S_L = \begin{pmatrix} -R & -1 & 0 & i \\ 1 & -1 & 1-R & 0 \\ R & R & 0 & -2iR \\ -1 & -1 & 0 & i \end{pmatrix}, \quad P_L = \begin{pmatrix} 0 & 0 & 1-R & 0 \\ 0 & 0 & 0 & -i/R \\ R & -1 & 0 & 0 \\ 0 & 0 & 0 & 0 \end{pmatrix}.$$

In matrix P_L, the fourth row only has null elements, $det\, P_L = 0$. The inverse matrix P_L^{-1} does not exist.

This suggests the degeneracy of the classic Landau's dynamics, and a singular and ill-posed character of the Landau-Darrieus instability. Eliminating this degeneracy may lead to appearance of a neutrally stable solution with a 'seed' vortical field, triggering the Landau-Darrieus instability. We address detailed consideration of this issue to the future.

Sub-section Comparative study

Table S1: Properties of the inertial conservative dynamics (CD) and the classic Landau-Darrieus (LD) dynamics in the linear regime

	CD	LD
Conservation properties	Conserves mass, momentum and energy at the interface	Conserves mass and momentum, has zero perturbed mass flux at the interface
Velocity of the interface as a whole	Slight stable oscillations near the constant value	Constant value (postulate)
Flow field	Potential velocity fields	Vortical structures in the light fluid
Inerfacial shear	Shear-free	Shear-free
Formal properties	Non-degenerate; 4 fundamental solutions and 4 degrees of freedom	Degenerate; 3 fundamental solutions and 4 degrees of freedom
Stability	Stable; stabilized by inertial effects	Unstable

Sub-section Mechanisms of stabilization and destabilization

a. Stabilization mechanism

Our work identifies a new stabilization mechanism of the conservative dynamics due to inertial effects that cause the reactive force to occur. In mechanics the 'reactive force' is also known as 'propulsion force'. It appears in inertial systems due to momentum conservation and it is the force that propels a rocket (hence the title).

Physically, the inertial effects are identified as a stabilization mechanism of the conservative dynamics on the basis of the following considerations. When the interface is slightly perturbed, the parcels of the heavy fluid and the light fluid follow the interface perturbation, thus causing the change of momentum and energy of the fluid system. Yet, the dynamics is inertial. To conserve the momentum and energy, the interface as a whole should slightly change its velocity. This causes the reactive force to occur and stabilize the dynamics, Figure S8.

Mathematically, slight oscillations of the interface as a whole are the property of the solution for the governing equations – the conservations of mass, momentum and energy. Our governing equations and their solution are derived in the inertial reference frame. This inertial reference frame can be referred to the reference frame moving with a constant velocity $\widetilde{\mathbf{V}}_0 = \left(0,0,\widetilde{V}_0\right)$ of the planar interface separating the fluids. If in the laboratory reference frame the heavy fluid is at rest, then the velocity of planar steady interface is $\widetilde{\mathbf{V}}_0 = -\mathbf{V}_h$, with $\widetilde{\mathbf{V}}_0 = \left(0,0,-V_h\right)$. In general case of the unsteady non-planar interface the velocity $\widetilde{\mathbf{V}}$ obeys the relation $\widetilde{\mathbf{V}}\cdot\mathbf{n} = -\mathbf{v}\cdot\mathbf{n}|_{\theta=0^+} = -\left(\widetilde{\mathbf{j}}/\rho\right)\cdot\mathbf{n}\big|_{\theta=0^+}$ and $\widetilde{\mathbf{V}} \neq \widetilde{\mathbf{V}}_0$. For a slightly perturbed dynamics, in the laboratory reference frame the interface velocity is $\widetilde{\mathbf{V}} = \widetilde{\mathbf{V}}_0 + \widetilde{\mathbf{v}}$ to the zeroth and first orders, with constant $\widetilde{\mathbf{V}}_0$ and with $\widetilde{\mathbf{v}}\cdot\mathbf{n}_0 = -\left(\mathbf{u}\cdot\mathbf{n}_0 + \dot{\theta}\right)\big|_{\theta=0^+}$, where $\mathbf{n}_0 = (0,0,-1)$.

For the conservative dynamics with solution $\mathbf{r}_{CD}$, the values are $\mathbf{u}\cdot\mathbf{n}_0\big|_{\theta=0^+} \sim e^{\pm i\sqrt{R}t}$ and $\dot{\theta}\big|_{\theta=0^+} \sim e^{\pm i\sqrt{R}t}$, leading to $\left(\mathbf{u}\cdot\mathbf{n}_0 + \dot{\theta}\right)\big|_{\theta=0^+} \sim e^{\pm i\sqrt{R}t}$ and $\widetilde{\mathbf{v}}\cdot\mathbf{n}_0 \sim e^{\pm i\sqrt{R}t}$. Thus, for the perturbed dynamics the velocity of the interface as a whole $\widetilde{\mathbf{V}} = \widetilde{\mathbf{V}}_0 + \widetilde{\mathbf{v}}$ experiences small stable oscillations near the steady value $\widetilde{\mathbf{V}}_0$ with $\left(\widetilde{\mathbf{V}} - \widetilde{\mathbf{V}}_0\right)\cdot\mathbf{n}_0 \sim e^{\pm i\sqrt{R}\,t}$, Figure S8.

The classic Landau's dynamics postulates the boundary condition $\left[\mathbf{u}\cdot\mathbf{n}_0\right] \equiv 0$, leading to the velocity to be constant $\widetilde{\mathbf{V}} \equiv \widetilde{\mathbf{V}}_0$ because $\widetilde{\mathbf{v}} \equiv 0$, associated with $\left(\mathbf{u}\cdot\mathbf{n}_0 + \dot{\theta}\right)\big|_{\theta=0^+} \equiv 0$ and with $\widetilde{\mathbf{v}}\cdot\mathbf{n}_0 = -\left(\mathbf{u}\cdot\mathbf{n}_0 + \dot{\theta}\right)\big|_{\theta=0^+} \equiv 0$. Note that while in the classic Landau's dynamics each of the terms

$\mathbf{u}\cdot\mathbf{n}_0\big|_{\theta=0^+} \sim e^{\omega_{LD}t}$ and $\dot{\theta}\big|_{\theta=0^+} \sim e^{\omega_{LD}t}$ grows exponentially in time, due to the condition $\left(\mathbf{u}\cdot\mathbf{n}_0+\dot{\theta}\right)\big|_{\theta=0^+} \equiv 0$, their combination is precisely balanced to zero, $\left(\mathbf{u}\cdot\mathbf{n}_0+\dot{\theta}\right)\big|_{\theta=0^+} \equiv 0$, Figure S8. The Landau's solution is a beautiful perfect match!

The difference in the boundary conditions leads to distinct interfacial dynamics. For the inertial conservative dynamics, the mass, momentum and energy are conserved in the bulk and at the interface. This flow is the superposition of two motions – the background motion of the fluids following the interface as a whole with the velocity slightly oscillating near its steady value, and the stable oscillations of the interface perturbations. For the Landau-Darrieus dynamics, the mass and momentum are conserved in the bulk and at the interface, and the normal component of the perturbed velocity is conserved at the interface, leading to the precise constancy of the velocity of the interface as a whole. This flow is the superposition of two motions – the background motion of the fluids following the interface with the constant velocity, and the growth of the interface perturbations, Figure S8.

In the presence of acceleration, the difference in the boundary conditions leads to the new hydrodynamic instability. Particularly, for the conservative dynamics, the velocity fields are potential in the bulk and are shear-free at the interface. The interface stability is set by the interplay of the inertia and buoyancy. The interface is unstable when the acceleration value exceeds a threshold. The growth-rate and the flow fields of this new instability differ quantitatively and qualitatively from those of the accelerated Landau-Darrieus instability and Rayleigh-Taylor instability. For large acceleration values, the new instability has the largest growth-rate.

In other hydrodynamic instabilities, such as the Richtmyer-Meshkov instability, one can also observe the flow as being the superposition of the two motions - the background motion of the fluids and the interface as a whole, and the growth of the interface perturbations [24,25].

b. Energy imbalance

For ideal incompressible fluids the solution $\mathbf{r}_{LD}$ for the classic Landau's dynamics is incompatible with the condition for energy balance at the perturbed interface [20]. Indeed, let us substitute the condition $[\mathbf{u}\cdot\mathbf{n}]=0$, or $j_n=0$, in the condition for energy balance $\left[J_n\left(w+(\mathbf{J}\cdot\mathbf{j})/\rho^2\right)\right]=0$. In this expression the scalar product term is $\mathbf{J}\cdot\mathbf{j}=J_n j_n+J_t j_t$ where J_t, j_t are respectively the zero-order and the perturbed components of the mass flux tangential to the interface. This term is zero, $\mathbf{J}\cdot\mathbf{j}=J_n j_n+J_t j_t=0$, because $J_t=0$ and $j_n=0$. Thus the balance equation is $\left[J_n\left(w+(\mathbf{J}\cdot\mathbf{j})/\rho^2\right)\right]=[J_n w]=0$, and, with $[J_n]=0$, it is reduced to $[w]=0$.

The energy imbalance can be scaled with kinetic energy $\sim V_h^2$, by presuming that $p \sim [\rho V^2]$, with $p \sim (\rho_l V_l^2 - \rho_h V_h^2)$ and $[w] = [p/\rho] \sim (\rho_l V_l^2 - \rho_h V_h^2)(1/\rho_l - 1/\rho_h)$, so that $[w] \sim V_h^2 (R-1)^2$. This scaling may be important for fluids with very different densities, $R \to \infty$. The energy imbalance can also be scaled zero-order enthalpy $\sim W_0$, as $[w] \sim W_0$. This scaling may be important for fluids with close densities, $R \sim 1^+$. Dimensionless parameter $\Pi = V_h^2 (R-1)^2 / W_0$, separates these two cases.

c. Conservative dynamics with energy fluctuations

The energy imbalance required for the Landau-Darrieus instability to develop can be induced by energy fluctuations. In realistic fluids, the effect of energy fluctuations can be self-consistently derived from entropy conditions with account for chemical reactions. In ideal fluids, to quantify the effect of energy imbalance on the interface stability, we introduce an additional artificial energy flux. The appropriate term may appear in the energy equation only to the first order, because the zeroth order changes are accounted for with the transformation $W_0 \to \widetilde{W}_0$. With modified first-order energy equation as $[J_n (w + (\mathbf{J} \cdot \mathbf{j})/2\rho^2) - j_n Q] = 0$, and with $Q_{h(l)} = q_{h(l)} V_h^2$, we obtain the conservative system with energy fluctuations matrix $\mathbf{M}$ is $\mathbf{M} = \widetilde{M}$:

$$\widetilde{M} = \begin{pmatrix} -R & -1 & -\omega + R\omega & i \\ 1 & -1 & 1-R & i\omega/R \\ R - R\omega & R + \omega & 0 & -2iR \\ q_h R + R\omega & q_l - R\omega & q_l\omega + R\omega - R^2\omega - q_h R\omega & i(-q_l + R^2) \end{pmatrix}$$

Its rank is 4. It has 4 eigenvalues ω_i and 4 eigenvectors $\mathbf{e}_i$. With $q_h - q_l = q$, its determinant is $det\,\widetilde{M} = i(R-1)^2(\omega - R)(\omega + R)(\omega^2 + R) + iq(\omega - R)((R+1)\omega^2 + 2R\omega - R(R-1))$. The parameter q, $q > 0$, describes the strength of energy fluctuations.

Note that $det\,\widetilde{M} = R\,det\,M - q(R/(R-1))det\,L$, where $q = q_h - q_l$. Thus, $det\,\widetilde{M} \to R\,det\,M$ for $q \to 0$ leading to the conservative dynamics, and $det\,\widetilde{M} \to -q(R/(R-1))det\,L$ for $q \to \infty$ leading to the Landau dynamics. For convenience, we scale $q = f(R-1)^2 R/(R+1)$ with constant f. The equation $det\,\widetilde{M} = 0$ takes the form

$$(\omega - R)[(\omega + R)(\omega^2 + R) + f(\omega^2 + \omega(2R/(R+1)) - (R(R-1)/(R+1)))R] = 0.$$

Figure S9 shows solutions for this equation – the eigenvalues ω_i with $i=1,2,3,4$ for a fixed R - as a function of f, illustrating the transition from the stable to unstable dynamics with the increase of the fluctuations strength f. For small f, $f=0.01$, values $\mathrm{Im}\left[\omega_{1(2)}\right]$ and $\omega_{3(4)}$ are indistinguishable from the corresponding values in the conservative dynamics. For large f, $f=100$, values ω_i with $i=1,2,3$ are indistinguishable from the corresponding values in the classic Landau system. The flow fields experience appropriate changes with the increase of fluctuations' strength.

d. Figure captions and Figures

Figure S8: Schematics of the flow dynamics in a far field approximation (not to scale) for the inertial conservative dynamics (left) and the classic Landau's dynamics (right) in the inertial reference frame. Blue color marks the planar interface (dashed) and the perturbed interface (solid). For the conservative dynamics the blue double arrows mark the oscillations of the interface perturbations (solid) and the interface velocity as a whole (dashed) with the latter occurring due to inertial effects and causing the reactive force to occur. For the classic Landau's dynamics the single blue arrows mark the growth of the interface perturbations; the velocity of the interface as a whole is postulated constant.

Figure S9: Dependence of eigenvalues ω_i, $i=1,2,3,4$, on f in a broad range of values f for conservative system with fluctuations. Density ratio is $R=5$.

Fig. S8

LD
CD
ρ_l
ρ_h
$\mathbf{V}_l$
$\mathbf{V}_h$
$\tilde{\mathbf{V}}_0$
z
x
$\mathbf{v}_l = \mathbf{V}_l + \mathbf{u}_l$
$\mathbf{v}_h = \mathbf{V}_h + \mathbf{u}_h$
$\tilde{\mathbf{V}} \equiv \tilde{\mathbf{V}}_0$
$\tilde{\mathbf{V}} = \tilde{\mathbf{V}}_0 + \tilde{\mathbf{v}}$
z^*

Fig. S9

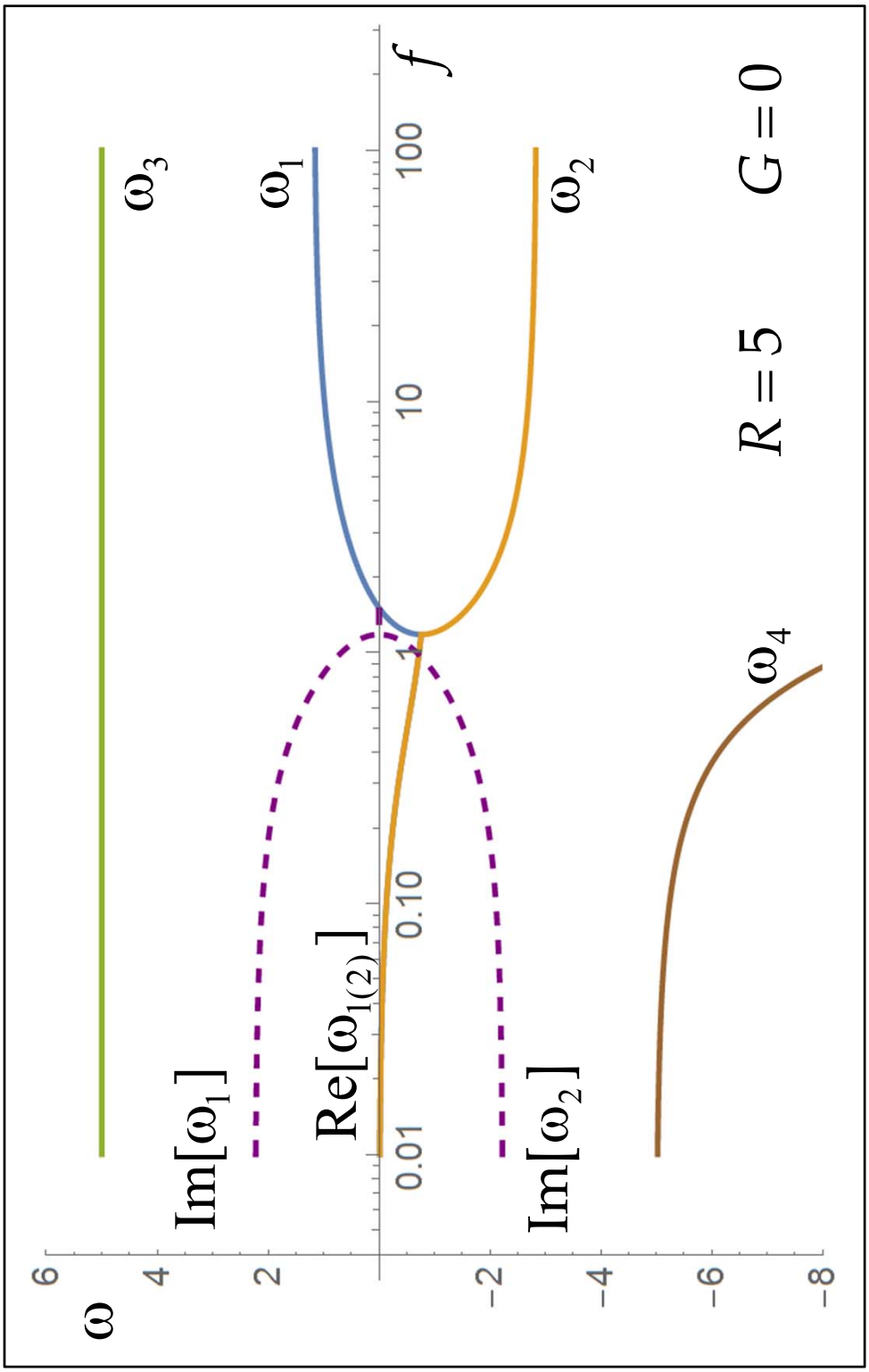

Section Results – Accelerated dynamics

Sub-section Accelerated conservative dynamics

a. Fundamental solutions

For the conservative dynamics, with $\mathrm{M}\,\mathbf{r} = 0$ and $\mathbf{r} = \left(\Phi_h, \Phi_l, V_h z^*, \Psi_l\right)$, the matrix $\mathrm{M} = M_G$ is

$$M_G = \begin{pmatrix} -R & -1 & -\omega + R\omega & i \\ 1 & -1 & 1-R & i\omega/R \\ R - R\omega & R+\omega & G(R-1) & -2iR \\ \omega & -\omega & \omega - R\omega & iR \end{pmatrix}.$$

Fundamental solution $\mathbf{r}_1(\omega_1, \mathbf{e}_1)$ has the eigenvalue ω_1 and eigenvector $\mathbf{e}_1$:

$$\omega_1 = \sqrt{\frac{-R(R-1)+G(R+1)}{R-1}}\ , \quad \mathbf{e}_1 = \begin{pmatrix} \dfrac{(R-1)+\sqrt{(R-1)(-R(R-1)+G(R+1))}}{R+1} \\ \dfrac{-R(R-1)+\sqrt{(R-1)(-R(R-1)+G(R+1))}}{R+1} \\ 1 \\ 0 \end{pmatrix}.$$

Fundamental solution $\mathbf{r}_2(\omega_2, \mathbf{e}_2)$ has the eigenvalue ω_2 and eigenvector $\mathbf{e}_2$:

$$\omega_2 = -\sqrt{\frac{-R(R-1)+G(R+1)}{R-1}}\ , \quad \mathbf{e}_2 = \begin{pmatrix} -\dfrac{-(R-1)+\sqrt{(R-1)(-R(R-1)+G(R+1))}}{R+1} \\ -\dfrac{R(R-1)+\sqrt{(R-1)(-R(R-1)+G(R+1))}}{R+1} \\ 1 \\ 0 \end{pmatrix}.$$

Fundamental solution $\mathbf{r}_3(\omega_3, \mathbf{e}_3)$ has the eigenvalue ω_3 and eigenvector $\mathbf{e}_3$:

$$\omega_3 = R\ , \quad \mathbf{e}_3 = \begin{pmatrix} 0 \\ i \\ 0 \\ 1 \end{pmatrix}.$$

Fundamental solution $\mathbf{r}_4(\omega_4, \mathbf{e}_4)$ has the eigenvalue ω_4 and eigenvector $\mathbf{e}_4$:

$$\omega_4 = -R\ , \quad \mathbf{e}_4 = \begin{pmatrix} \dfrac{2i}{1+R} \\ -\dfrac{i(R-1)}{1+R} \\ 0 \\ 1 \end{pmatrix}.$$

Sub-section Accelerated Landau-Darrieus dynamics

a. Fundamental solutions

For accelerated Landau's dynamics, with $\mathrm{M}\,\mathbf{r}=0$ and $\mathbf{r}=\left(\Phi_h,\Phi_l,V_h z^*,\Psi_l\right)$, matrix $\mathrm{M}=L_G$ is

$$L_G=\begin{pmatrix} -R & -1 & -\omega+R\omega & i \\ 1 & -1 & 1-R & i\omega/R \\ R-R\omega & R+\omega & G(R-1) & -2iR \\ -1 & -1 & 0 & i \end{pmatrix}$$

Fundamental solution $\mathbf{r}_1(\omega_1,\mathbf{e}_1)$ has the eigenvalue ω_1 and eigenvector $\mathbf{e}_1$:

$$\omega_1=\frac{-R+\sqrt{\left(R^3+R^2-R\right)+G\left(R^2-1\right)}}{1+R},$$

$$\mathbf{e}_1=\begin{pmatrix} i\dfrac{\left(R-\sqrt{R\left(R^2+R-1\right)+G\left(R^2-1\right)}\right)\left(\left(R^2+2R\right)-\sqrt{R\left(R^2+R-1\right)+G\left(R^2-1\right)}\right)}{R(R+1)\left(\left(R^2+2R-1\right)-2\sqrt{R\left(R^2+R-1\right)+G\left(R^2-1\right)}\right)} \\ -i\dfrac{(R-1)\left(R\left(\sqrt{R\left(R^2+R-1\right)+G\left(R^2-1\right)}-\left(R^2+2R\right)\right)+G(R+1)\right)}{R(R+1)\left(\left(R^2+2R-1\right)-2\sqrt{R\left(R^2+R-1\right)+G\left(R^2-1\right)}\right)} \\ -i\dfrac{\left(\left(R^2+2R\right)-\sqrt{R\left(R^2+R-1\right)+G\left(R^2-1\right)}\right)}{R\left(\left(R^2+2R-1\right)-2\sqrt{R\left(R^2+R-1\right)+G\left(R^2-1\right)}\right)} \\ 1 \end{pmatrix}.$$

Fundamental solution $\mathbf{r}_2(\omega_2,\mathbf{e}_2)$ has the eigenvalue ω_2 and eigenvector $\mathbf{e}_2$:

$$\omega_2=\frac{-R-\sqrt{\left(R^3+R^2-R\right)+G\left(R^2-1\right)}}{1+R},$$

$$\mathbf{e}_2=\begin{pmatrix} i\dfrac{\left(R+\sqrt{R\left(R^2+R-1\right)+G\left(R^2-1\right)}\right)\left(\left(R^2+2R\right)+\sqrt{R\left(R^2+R-1\right)+G\left(R^2-1\right)}\right)}{R(R+1)\left(\left(R^2+2R-1\right)+2\sqrt{R\left(R^2+R-1\right)+G\left(R^2-1\right)}\right)} \\ -i\dfrac{(R-1)\left(R\left(\sqrt{R\left(R^2+R-1\right)+G\left(R^2-1\right)}+\left(R^2+2R\right)\right)-G(R+1)\right)}{R(R+1)\left(\left(R^2+2R-1\right)+2\sqrt{R\left(R^2+R-1\right)+G\left(R^2-1\right)}\right)} \\ -i\dfrac{\left(\left(R^2+2R\right)+\sqrt{R\left(R^2+R-1\right)+G\left(R^2-1\right)}\right)}{R\left(\left(R^2+2R-1\right)+2\sqrt{R\left(R^2+R-1\right)+G\left(R^2-1\right)}\right)} \\ 1 \end{pmatrix}.$$

Fundamental solution $\mathbf{r}_3(\omega_3,\mathbf{e}_3)$ has the eigenvalue ω_3 and eigenvector $\mathbf{e}_3$:

$$\omega_3=R\ ,\quad \mathbf{e}_3=\begin{pmatrix} 0 \\ i \\ 0 \\ 1 \end{pmatrix}$$

b. Figure captions and Figures

Figure S10: Flow fields' structure for the accelerated Landau's dynamics, fundamental solution $\mathbf{r}_{LDG}\left(\omega_{LDG},\mathbf{e}_{LDG}\right)$ with $\mathbf{r}_{LDG}=\mathbf{r}_1$ (a) Plots of the perturbed velocity vector fields $\mathbf{u}_{h(l)}$, the perturbed velocity streamlines $\mathbf{s}_{h(l)}$, the contour plot of the perturbed pressure $p_{h(l)}$, and the interface perturbation z^* in (x,z) plane. (b) Plots of the perturbed velocity vortical component $\nabla\times\boldsymbol{\Psi}_l$, the contour plot of vorticity $\nabla\times\mathbf{u}_l$, and the interface perturbation z^* in the (x,z) plane. Gravity value is $G=\left(G^*+G_{cr}\right)/2$, with $G_{cr}=R(R-1)/(R+1)$ and $G^*=\left(R^2-1\right)/4$. Density ratio is $R=5$, gravity value is $G=14/3$, time is $t=\pi/2$, $[t]=1/kV_h$. The values are $|p_l|_{\max(\min)}/|p_h|_{\max(\min)}\approx 1/5$. Red (blue) marks positive (negative) values in contour plots. Real parts of fields and functions are shown.

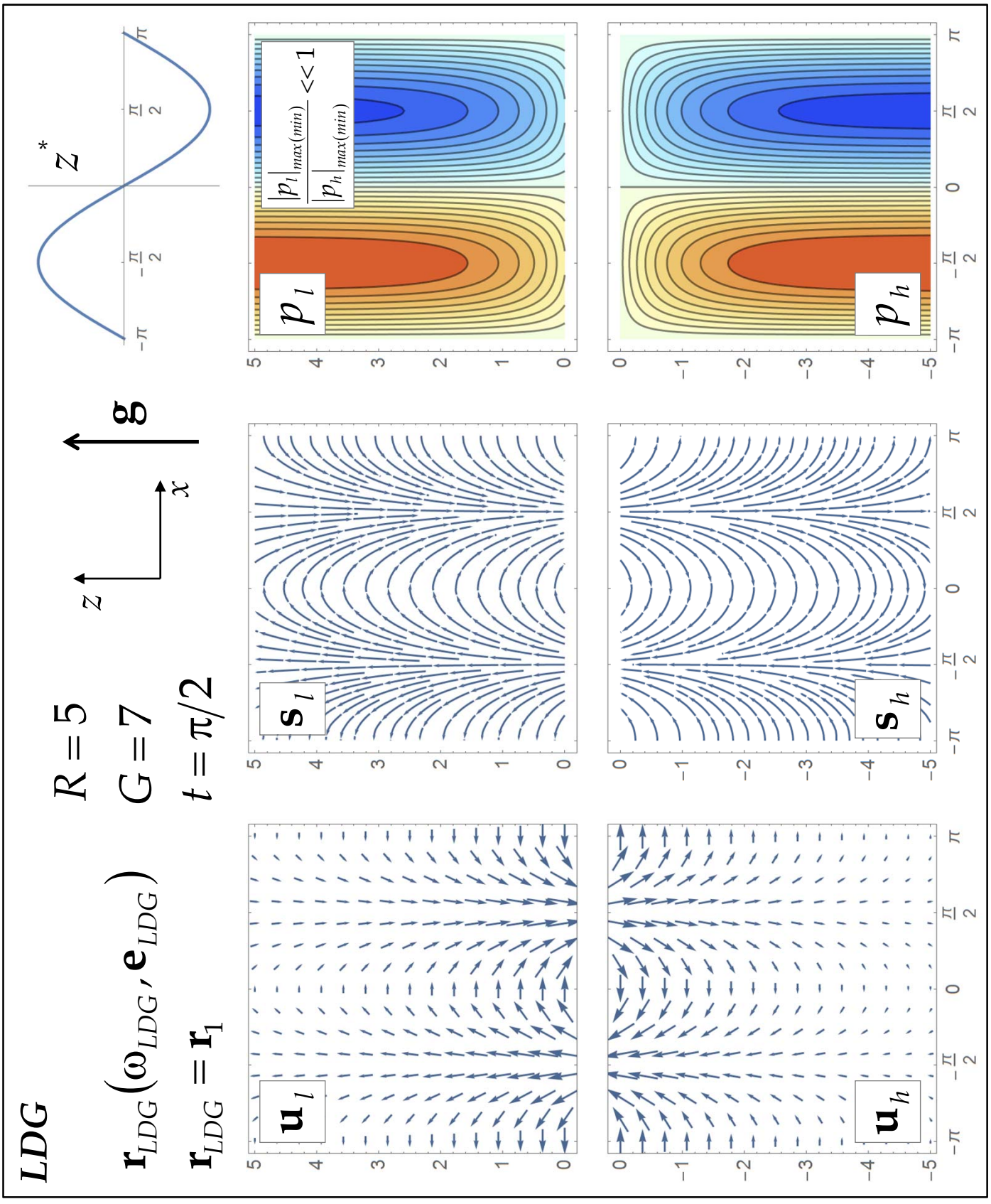
LDG
$\mathbf{r}_{LDG}\left(\omega_{LDG}, \mathbf{e}_{LDG}\right)$
$\mathbf{r}_{LDG} = \mathbf{r}_1$
$R = 5$
$G = 7$
$t = \pi/2$
z
x
g
z^*
$\mathbf{u}_l$
$\mathbf{s}_l$
p_l
$\frac{|p_l|_{max(min)}}{|p_h|_{max(min)}} << 1$
$\mathbf{u}_h$
$\mathbf{s}_h$
p_h

Fig. S10a

Fig. S10b

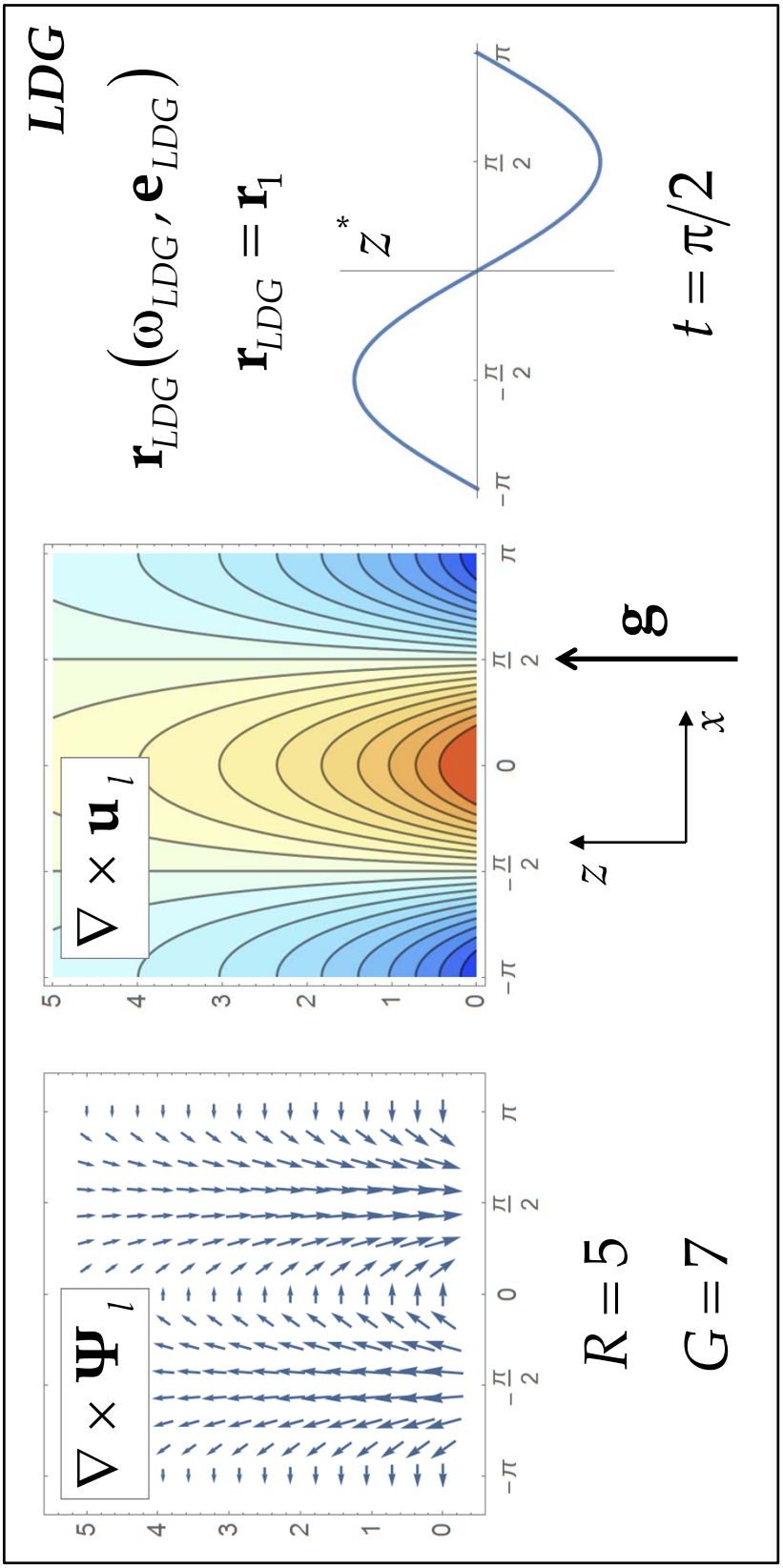
LDG
$\mathbf{r}_{LDG}(\omega_{LDG}, \mathbf{e}_{LDG})$
$\mathbf{r}_{LDG} = \mathbf{r}_1$
Z^*
$t = \pi/2$
$\nabla \times \mathbf{u}_l$
$\nabla \times \boldsymbol{\Psi}_l$
$\mathbf{g}$
z
x
$R = 5$
$G = 7$

Sub-section Accelerated Rayleigh-Taylor dynamics

a. Fundamental solutions

For the Rayleigh-Taylor dynamics, with $\mathrm{M}\,\mathbf{r}=0$ and $\mathbf{r}=\left(\Phi_h,\Phi_l,V_h z^*\right)$, the matrix $\mathrm{M}=T_G$ is

$$T_G=\begin{pmatrix} -R & -1 & -\omega+R\omega \\ -R-R\omega & -R+\omega & G(R-1) \\ -1 & -1 & 0 \end{pmatrix}.$$

Fundamental solution $\mathbf{r}_1\left(\omega_1,\mathbf{e}_1\right)$ has the eigenvalue ω_1 and eigenvector $\mathbf{e}_1$:

$$\omega_1=\sqrt{G\frac{R-1}{R+1}}\ ,\ \mathbf{e}_1=\begin{pmatrix} \sqrt{G\frac{R-1}{R+1}} \\ -\sqrt{G\frac{R-1}{R+1}} \\ 1 \end{pmatrix}.$$

Fundamental solution $\mathbf{r}_2\left(\omega_2,\mathbf{e}_2\right)$ has the eigenvalue ω_2 and eigenvector $\mathbf{e}_2$:

$$\omega_2=-\sqrt{G\frac{R-1}{R+1}}\ ,\ \mathbf{e}_2=\begin{pmatrix} -\sqrt{G\frac{R-1}{R+1}} \\ \sqrt{G\frac{R-1}{R+1}} \\ 1 \end{pmatrix}.$$

b. Figure captions and Figures

Figure S11: Flow fields' structure for the Rayleigh-Taylor dynamics, fundamental solution $\mathbf{r}_{RT}\left(\omega_{RT},\mathbf{e}_{RT}\right)$ with $\mathbf{r}_{RT}=\mathbf{r}_1$. Plots of the perturbed velocity vector fields $\mathbf{v}_{h(l)}$, the perturbed velocity streamlines $\mathbf{s}_{h(l)}$, and the contour plot of the perturbed pressure $p_{h(l)}$, and the interface perturbation z^* in the (x,z) plane. The velocity vortical component is $\nabla\times\boldsymbol{\Psi}_l=0$ and vorticity is $\nabla\times\mathbf{v}_{h(l)}=0$. Gravity value is $G=(3/2)\left(G^*+G_{cr}\right)$, with $G_{cr}=R(R-1)/(R+1)$ and $G^*=\left(R^2-1\right)/4$. Density ratio is $R=5$, gravity value is $G=7$, time is $t=\pi/2$, $[t]=1/kV_h$. The values are $\left|p_l\right|_{\max(\min)}/\left|p_h\right|_{\max(\min)}\approx 1/5$. Red (blue) marks positive (negative) values in contour plots. Real parts of fields and functions are shown.

Fig. S11

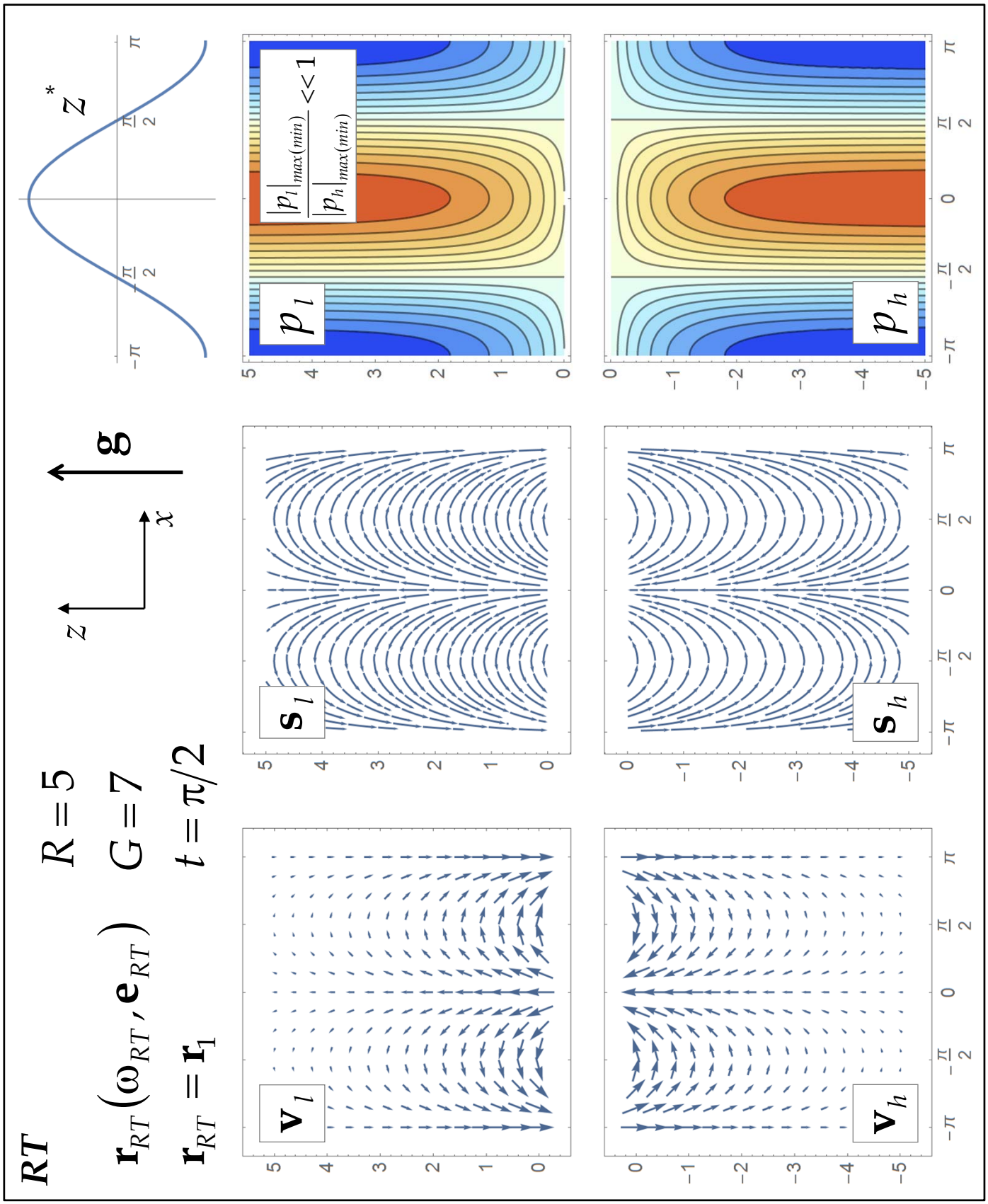
RT
$\mathbf{r}_{RT}\left(\omega_{RT}, \mathbf{e}_{RT}\right)$
$R=5$
$G=7$
$\mathbf{r}_{RT}=\mathbf{r}_1$
$t=\pi/2$
z
x
g
z^*
$\mathbf{v}_l$
$\mathbf{s}_l$
p_l
$\frac{|p_l|_{max(min)}}{|p_h|_{max(min)}} << 1$
$\mathbf{v}_h$
$\mathbf{s}_h$
p_h

c. Degenerate character of Rayleigh-Taylor dynamics

For Rayleigh-Taylor dynamics, for matrix $\mathrm{M} = T_G$, the associated matrices $\mathrm{S} = S_{T_G}$ and $\mathrm{P} = P_{T_G}$ are

$$S_{T_G} = \begin{pmatrix} -R & -1 & 0 \\ -R & -R & G(R-1) \\ -1 & -1 & 0 \end{pmatrix}, \; P_{T_G} = \begin{pmatrix} 0 & 0 & 1-R \\ R & -1 & 0 \\ 0 & 0 & 0 \end{pmatrix}$$

Determinant $det\, P_{T_G} = 0$, the inverse matrix $P_{T_G}^{-1}$ does not exist.

This suggests the degeneracy of the dynamics, and a singular and ill-posed character of the RTI. Eliminating this degeneracy may produce a neutrally stable solution with a 'seed' velocity shear at the fluid interface, triggering the RTI. We address detailed consideration of this issue to the future.

Sub-section Comparative study

a. Properties of the growth-rates of the instabilities

Table S2: Properties of growth-rates of the new conservative dynamics instability ω_{CDG} , the Landau-Darrieus instability ω_{LDG} , and the Rayleigh-Taylor instability ω_{RT} in gravity field G, $G \in (0,+\infty)$.

	$G \to 0$	$0 < G < G_{cr}$	$G_{cr} < G < G^*$	$G > G^*$	$G \to \infty$
$\mathrm{Re}[\omega_{CDG}]$	0	0	>0, $\omega_{CDG} < \omega_{LDG}$	>0, $\omega_{CDG} > \omega_{LDG}$	$\sqrt{RG/G_{cr}}$
$\mathrm{Re}[\omega_{RT}]$	0	>0	>0, $\omega_{CDG} < \omega_{RT}$	>0, $\omega_{CDG} > \omega_{RT}$	ω_{RT}
$\mathrm{Re}[\omega_{LDG}]$	>0	>0	>0, $\omega_{RT} < \omega_{LDG}$	>0, $\omega_{RT} > \omega_{LDG}$	ω_{RT}

Here $\omega_{CDG} = i\sqrt{R}\sqrt{1-\frac{G}{G_{cr}}}$, $\omega_{LDG} = \frac{-R+\sqrt{\left(R^3+R^2-R\right)+G\left(R^2-1\right)}}{1+R}$, $\omega_{RT} = \sqrt{G\frac{R-1}{1+R}}$,

$G_{cr} = R\frac{R-1}{R+1}$, $G^* = \frac{R^2-1}{4}$.

b. Properties of the accelerated instabilities

Table S3: Properties of the accelerated conservative dynamics (CDG), accelerated Landau-Darrieus (LDG) dynamics and Rayleigh-Taylor (RT) dynamics in the linear regime

	CDG	LDG	RT
Conservation properties	Conserves mass, momentum and energy at the interface	Conserves mass and momentum and has zero perturbed mass flux at the interface	Conserves mass and momentum and has zero mass flux at the interface
Interface velocity of the as a whole	Time-dependent	Constant	Zero
Flow field	Potential velocity fields	Vortical structures in the light fluid	Potential velocity fields
Interfacial shear	Shear-free	Shear-free	Interfacial shear
Formal properties	Non-degenerate; 4 fundamental solutions and 4 degrees of freedom	Degenerate; 3 fundamental solutions and 4 degrees of freedom	Degenerate; 2 fundamental solutions and 3 degrees of freedom
Stability	Stability is set by the interplay of effects of inertia (reactive force) and buoyancy (gravity). Stable for small gravity values below threshold; unstable for large gravity value above threshold; largest growth-rate for large gravity values	Unstable for any gravity value, including zero gravity value; largest growth-rate for small gravity values; smallest growth-rate for large gravity values	Unstable for any gravity value, neutrally stable for zero gravity

Sub-section Mechanism of stabilization and destabilization

a. Critical and maximum wavevector values

For accelerated conservative dynamics the interface stability is defined by the interplay of the effect of inertia and buoyancy (i.e., the reactive force and gravity). The eigenvalue is $\omega_{CDG} = \sqrt{R}\sqrt{G/G_{cr} - 1}$. For small acceleration values, $G/G_{cr} < 1$, the inertial effects dominate and the dynamics is stable, $\omega_{CDG} = i\sqrt{R}\sqrt{1 - G/G_{cr}}$. For large acceleration values, $G/G_{cr} > 1$, buoyancy effects dominate and the dynamics is unstable $\omega_{CDG} = \sqrt{R}\sqrt{G/G_{cr} - 1}$.

In dimensional units the growth-rate value is $\Omega = (kV_h)\omega$, and the gravity value is $g = (kV_h^2)G$. For fixed values of $V_h, g, \sigma, \rho_h, \rho_l$, we find the critical wavevector k_{cr} at which the interface is stabilized from the condition $\Omega_{CDG}\big|_{k=k_{cr}} = 0$. We further find the maximum wavevector k_{max} at which the unstable interface has the fastest growth from the conditions $\partial\Omega_{CDG}/\partial k\big|_{k=k_{max}} = 0, \partial^2\Omega_{CDG}/\partial k^2\big|_{k=k_{max}} < 0$.

Table S4: For the accelerated conservative dynamics with fixed values of $V_h, g, \sigma, \rho_h, \rho_l$, the values of the critical wavevector k_{cr}, at which the interface is stabilized, and the maximum wavevector k_{max} at which the unstable interface has the fastest growth. The ratio is $(k_{cr}/k_{max}) = 2$.

Critical wavevector	$k_{cr} = \left(\frac{g}{V_h^2}\right)\left(\frac{\rho_l}{\rho_h}\right)\left(\frac{\rho_h + \rho_l}{\rho_h - \rho_l}\right)$
Maximum wavevector	$k_{max} = \frac{1}{2}\left(\frac{g}{V_h^2}\right)\left(\frac{\rho_l}{\rho_h}\right)\left(\frac{\rho_h + \rho_l}{\rho_h - \rho_l}\right)$

Sub-section Effect of surface tension

a. Formalism

Our general framework enables systematic study of interfacial dynamics influenced by surface tension, thermal conductivity, compressibility, viscosity, mass ablation, and flow geometry and dimensionality, upon the corresponding modification of the governing equations. Here we briefly consider the effect of surface tension. It is important in multi-phase flows, and is straightforward to account for. Physically, for interfacial dynamics with interfacial mass flux, surface tension can be viewed as a tension at the phase boundary between the flow phases. Mathematically, surface tension contributes to the dynamics with an additional term modifying the pressure perturbation in the governing equations as $\left(p_h - p_l\right) \to \left(p_h - p_l\right) + \sigma\left(\partial^2 z^* / \partial x^2\right)$.

For the inertial dynamics with the dimensionless surface tension $T = \left(\sigma/\rho_h\right)\left(k/V_h^2\right)$, the associated eigenvalues are $\hat{\omega}_{CD}$, $\hat{\omega}_{LD}$, $\hat{\omega}_{RT}\big|_{G=0}$ for the conservative dynamics, Landau-Darrieus dynamics and Rayleigh-Taylor dynamics, respectively:

$$\hat{\omega}_{CD} = i\sqrt{R}\sqrt{1 + T/(R-1)},\ \hat{\omega}_{LD} = \left(-R + \sqrt{\left(R^3 + R^2 - R\right) - TR(R+1)}\right)\Big/(1+R),$$
$$\hat{\omega}_{RT}\big|_{G=0} = i\sqrt{T\,R/(R+1)} \qquad \text{(SI-2a)}$$

where $\hat{\omega}_{RT}\big|_{G=0}$ is understood as the frequency of the capillary wave [5]. The conservative dynamics $\hat{\omega}_{CD}$ and capillary wave dynamics $\hat{\omega}_{RT}\big|_{G=0}$ are stable for $T > 0$; Landau-Darrieus dynamics $\hat{\omega}_{LD}$ is stable for $T > R - 1$.

For the accelerated dynamics with surface tension T, the associated eigenvalues are $\hat{\omega}_{CDG}$, $\hat{\omega}_{LDG}$, $\hat{\omega}_{RT}$ for the accelerated conservative dynamics and the accelerated Landau-Darrieus and Rayleigh-Taylor dynamics, respectively:

$$\hat{\omega}_{CDG} = \sqrt{R}\sqrt{\widetilde{G}/G_{cr} - 1},\ \hat{\omega}_{LDG} = \left(-R + \sqrt{\left(R^3 + R^2 - R\right) + \overline{G}\left(R^2 - 1\right)}\right)\Big/(1+R),$$
$$\hat{\omega}_{RT} = \sqrt{\overline{G}\,(R-1)/(R+1)} \qquad \text{(SI-2b)}$$

where $\widetilde{G} = G - T\,R/(R+1)$ and $\overline{G} = G - T\,R/(R-1)$. The accelerated conservative dynamics $\hat{\omega}_{CDG}$ is stable for $T > \left(G - G_{cr}\right)(R+1)/R$. The accelerated LD dynamics $\hat{\omega}_{LDG}$ is stable for $T > (G+R)(R-1)/R$; RT dynamics $\hat{\omega}_{RT}$ is stable for $T > G(R-1)/R$.

b. Matrices

In the presence of gravity G and surface tension T the matrices for the conservative dynamics $\hat{M}_G$, Landau's dynamics $\hat{L}_G$ and Rayleigh-Taylor dynamics $\hat{T}_G$ have the form:

$$\hat{M}_G = \begin{pmatrix} -R & -1 & -\omega + R\omega & i \\ 1 & -1 & 1-R & i\omega/R \\ R - R\omega & R+\omega & G(R-1) - RT & -2iR \\ \omega & -\omega & T + \omega - R\omega & iR \end{pmatrix}$$

$$\hat{L}_G = \begin{pmatrix} -R & -1 & -\omega + R\omega & i \\ 1 & -1 & 1-R & i\omega/R \\ R - R\omega & R+\omega & G(R-1) - RT & -2iR \\ -1 & -1 & 0 & i \end{pmatrix}$$

$$\hat{T}_G = \begin{pmatrix} -R & -1 & -\omega + R\omega \\ -R - R\omega & -R+\omega & G(R-1) - RT \\ -1 & -1 & 0 \end{pmatrix}$$

c. Eigenvalues

Table S5: Eigenvalues for the conservative dynamics $\hat{\omega}_{CD}$, the classic Landau's dynamics $\hat{\omega}_{LD}$, and the Rayleigh-Taylor dynamics $\hat{\omega}_{RT}\big|_{G=0}$ in the presence of surface tension T at zero gravity $G=0$, and the associated stability intervals. The eigenvalue $\hat{\omega}_{RT}\big|_{G=0}$ is frequency of capillary wave.

Dynamics	Eigenvalue	Stability interval
CD	$\hat{\omega}_{CD} = i\sqrt{R}\sqrt{1+T/(R-1)}$	$T>0$
LD	$\hat{\omega}_{LD} = \left(-R+\sqrt{\left(R^3+R^2-R\right)-TR(R+1)}\right)/(1+R)$	$T>(R-1)$
RT	$\hat{\omega}_{RT}\big\|_{G=0} = i\sqrt{T\,R/(R+1)}$	$T>0$

Table S6: Eigenvalues for the accelerated conservative dynamics $\hat{\omega}_{CDG}$, the accelerated Landau's dynamics $\hat{\omega}_{LDG}$, and the Rayleigh-Taylor dynamics $\hat{\omega}_{RT}$ in the presence of surface tension T and gravity G, and the associated stability intervals.

Dynamics	Eigenvalue	Stability interval
CDG	$\hat{\omega}_{CDG} = \sqrt{R}\sqrt{\widetilde{G}/G_{cr}-1}$	$T>(G-G_{cr})(R+1)/R$
LDG	$\hat{\omega}_{LDG} = \left(-R+\sqrt{\left(R^3+R^2-R\right)+\overline{G}\left(R^2-1\right)}\right)/(1+R)$	$T>(G+R)(R-1)/R$
RT	$\hat{\omega}_{RT} = \sqrt{\overline{G}\,(R-1)/(R+1)}$	$T>G(R-1)/R$

Here the values are $\widetilde{G}=G-T\,R/(R+1)$, $\overline{G}=G-T\,R/(R-1)$, $G_{cr}=R(R-1)/(R+1)$.

d. Critical and maximum wavevector values

In dimensional units, for fixed values $V_h, g, \sigma, \rho_h, \rho_l$, we can find wavevector(s) $k_{cr(max)}$, at which the interface is stable (the instability has the fastest growth). The outline of results is given below. The details the dependence of $k_{cr(max)}$ on $V_h, g, \sigma, \rho_h, \rho_l$. will be discussed elsewhere. Note that stabilization of the conservative dynamics by the inertial effect and by the surface tension are distinct mechanisms.

Table S7: The critical wavevector k_{cr} at which the interface is stabilized in the presence of gravity and surface tension for the accelerated conservative dynamics, the accelerated Landau's dynamics, and the Rayleigh-Taylor dynamics for fixed values of $V_h, g, \sigma, \rho_h, \rho_l$.

Dynamics	Critical wavevector
CDG	$\frac{1}{2\sigma}\left[-V_h^2\left(\frac{\rho_h}{\rho_l}\right)(\rho_h-\rho_l)+\sqrt{4\sigma g(\rho_h+\rho_l)+\left(V_h^2\left(\frac{\rho_h}{\rho_l}\right)(\rho_h-\rho_l)\right)^2}\right]$
LDG	$\frac{1}{2\sigma}\left[-V_h^2\left(\frac{\rho_h}{\rho_l}\right)(\rho_h-\rho_l)+\sqrt{4\sigma g(\rho_h-\rho_l)+\left(V_h^2\left(\frac{\rho_h}{\rho_l}\right)(\rho_h-\rho_l)\right)^2}\right]$
RT	$\sqrt{\frac{g}{\sigma}(\rho_h-\rho_l)}$

Table S8: The maximum wavevector k_{max} at which the unstable interface has the fastest growth in the presence of gravity and surface tension for the accelerated conservative dynamics, and the Rayleigh-Taylor dynamics for fixed values of $V_h, g, \sigma, \rho_h, \rho_l$. For the accelerated Landau-Darrieus dynamics, the dependence of k_{max} on the (fixed) values $V_h, g, \sigma, \rho_h, \rho_l$ is cumbersome; we discuss it elsewhere.

Dynamics	Maximum wavevector
CDG	$\frac{1}{6\sigma}\left[-2V_h^2\left(\frac{\rho_h}{\rho_l}\right)(\rho_h-\rho_l)+\sqrt{12\sigma g(\rho_h+\rho_l)+\left(2V_h^2\left(\frac{\rho_h}{\rho_l}\right)(\rho_h-\rho_l)\right)^2}\right]$
RT	$\frac{1}{\sqrt{3}}\sqrt{\frac{g}{\sigma}(\rho_h-\rho_l)}$

Section Figures

Captions and Figures 1-7

Figure 1: Dependence of eigenvalues on density ratio; (A) Conservative dynamics. (B) Classic Landau dynamics.

Figure 2: Flow fields' structure for the inertial conservative dynamics. Plots of real parts of the interface perturbation, the perturbed velocity vector fields, the perturbed velocity streamlines, and the contour plot of the perturbed pressure with red (blue) for positive (negative) values.

Figure 3: Flow fields' structure for the classic Landau's dynamics. Plots of real parts of the interface perturbation, the perturbed velocity vector fields, the perturbed velocity streamlines, and the contour plot of the perturbed pressure with red (blue) for positive (negative) values.

Figure 4: Dependence of eigenvalues on density ratio at some gravity value. (A) Accelerated conservative dynamics. (B) Accelerated Landau dynamics.

Figure 5: Flow fields' structure for the accelerated conservative dynamics. Plots of real parts of the interface perturbation, perturbed velocity vector fields, perturbed velocity streamlines, and contour plot of perturbed pressure with red (blue) for positive (negative) values.

Figure 6: Flow fields' structure for the accelerated Landau's dynamics. Plots of real parts of the interface perturbation, the perturbed velocity vector fields, the perturbed velocity streamlines, and contour plot of perturbed pressure with red (blue) for positive (negative) values.

Figure 7: Dependence of the growth rates of the instabilities on gravity value.

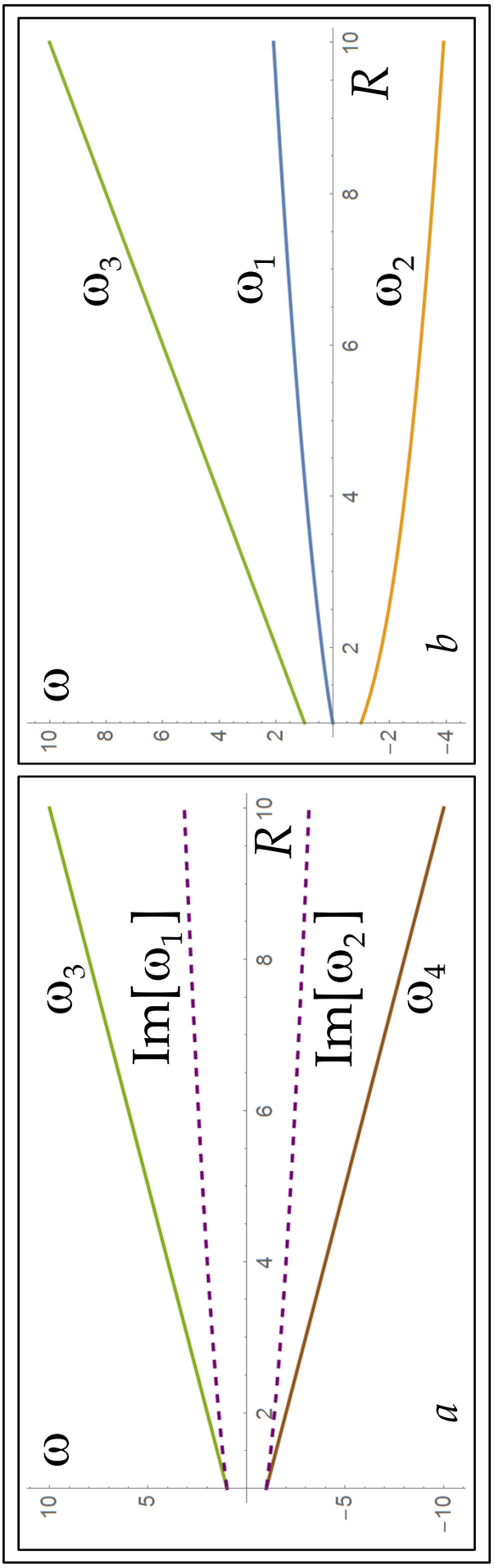
ω
10
8
6
4
2
−2
−4
2
4
6
8
10
R
ω3
ω1
ω2
b
ω
10
5
2
4
6
8
10
R
−5
−10
ω3
Im[ω1]
Im[ω2]
ω4
a

Fig.1

Fig.2

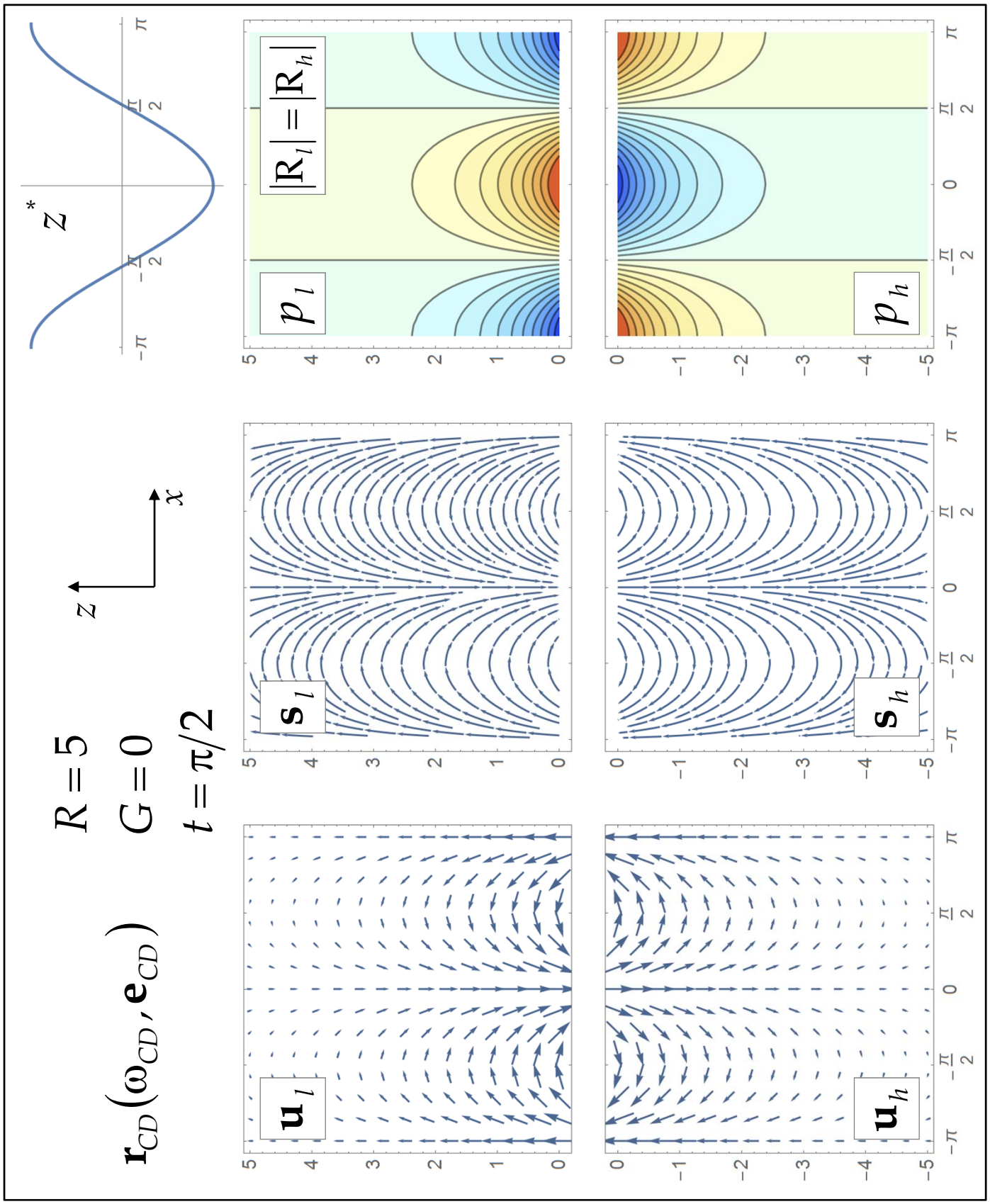
$\mathbf{r}_{CD}(\omega_{CD}, \mathbf{e}_{CD})$
$R = 5$
$G = 0$
$t = \pi/2$
z
x
Z^*
$|\mathrm{R}_l| = |\mathrm{R}_h|$
p_l
p_h
$\mathbf{s}_l$
$\mathbf{s}_h$
$\mathbf{u}_l$
$\mathbf{u}_h$

Fig.3

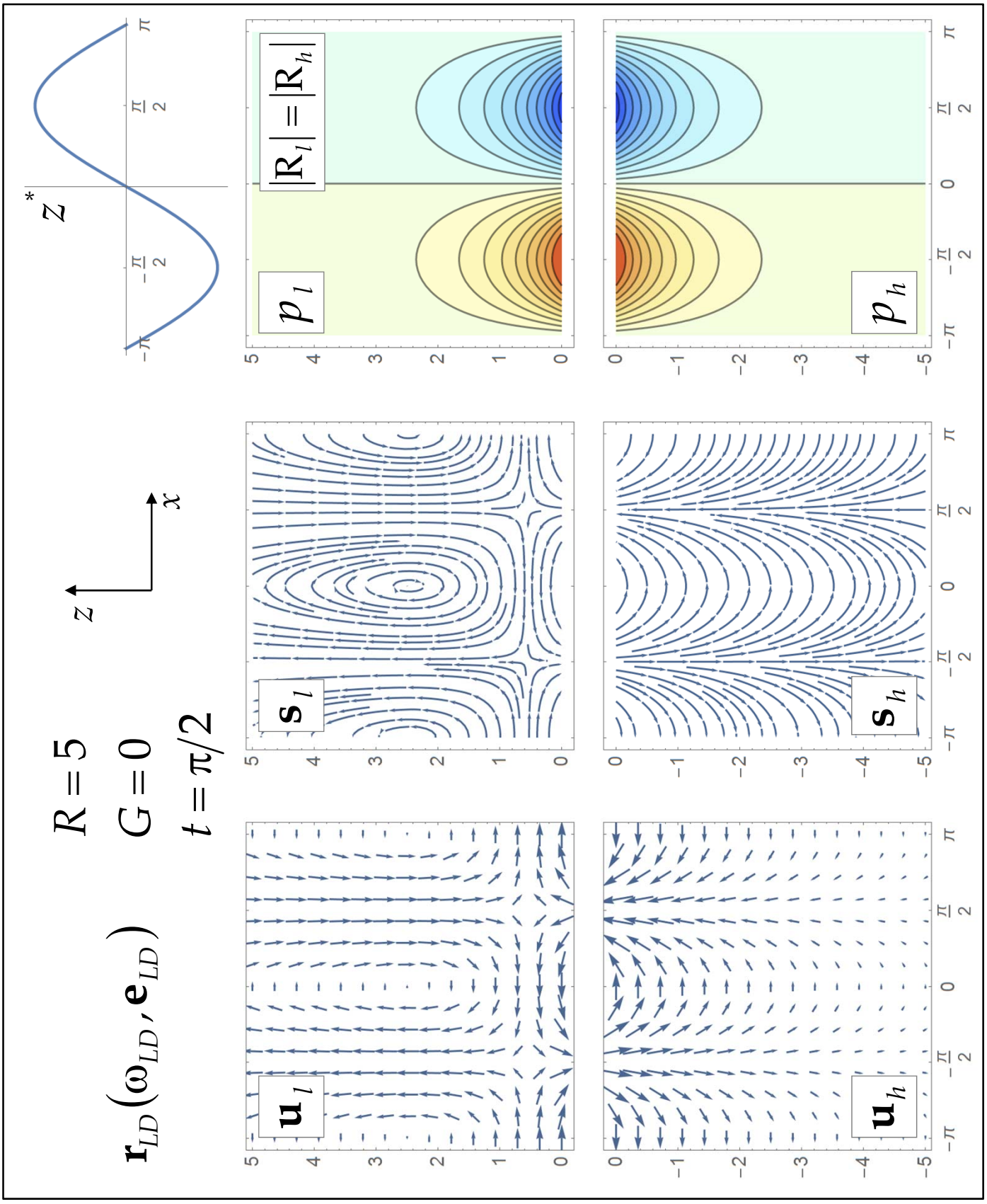
$\mathbf{r}_{LD}(\omega_{LD}, \mathbf{e}_{LD})$
$R = 5$
$G = 0$
$t = \pi/2$
z
x
z^*
$\mathbf{u}_l$
$\mathbf{s}_l$
p_l
$|\mathrm{R}_l| = |\mathrm{R}_h|$
$\mathbf{u}_h$
$\mathbf{s}_h$
p_h

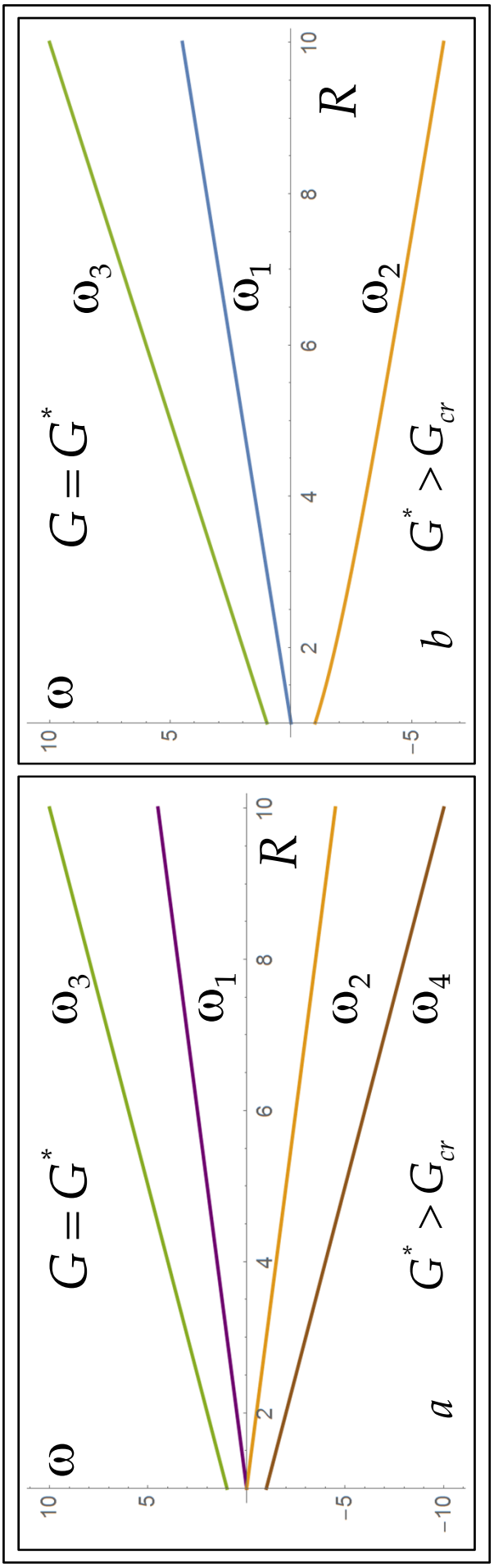

Fig.4

Fig.5

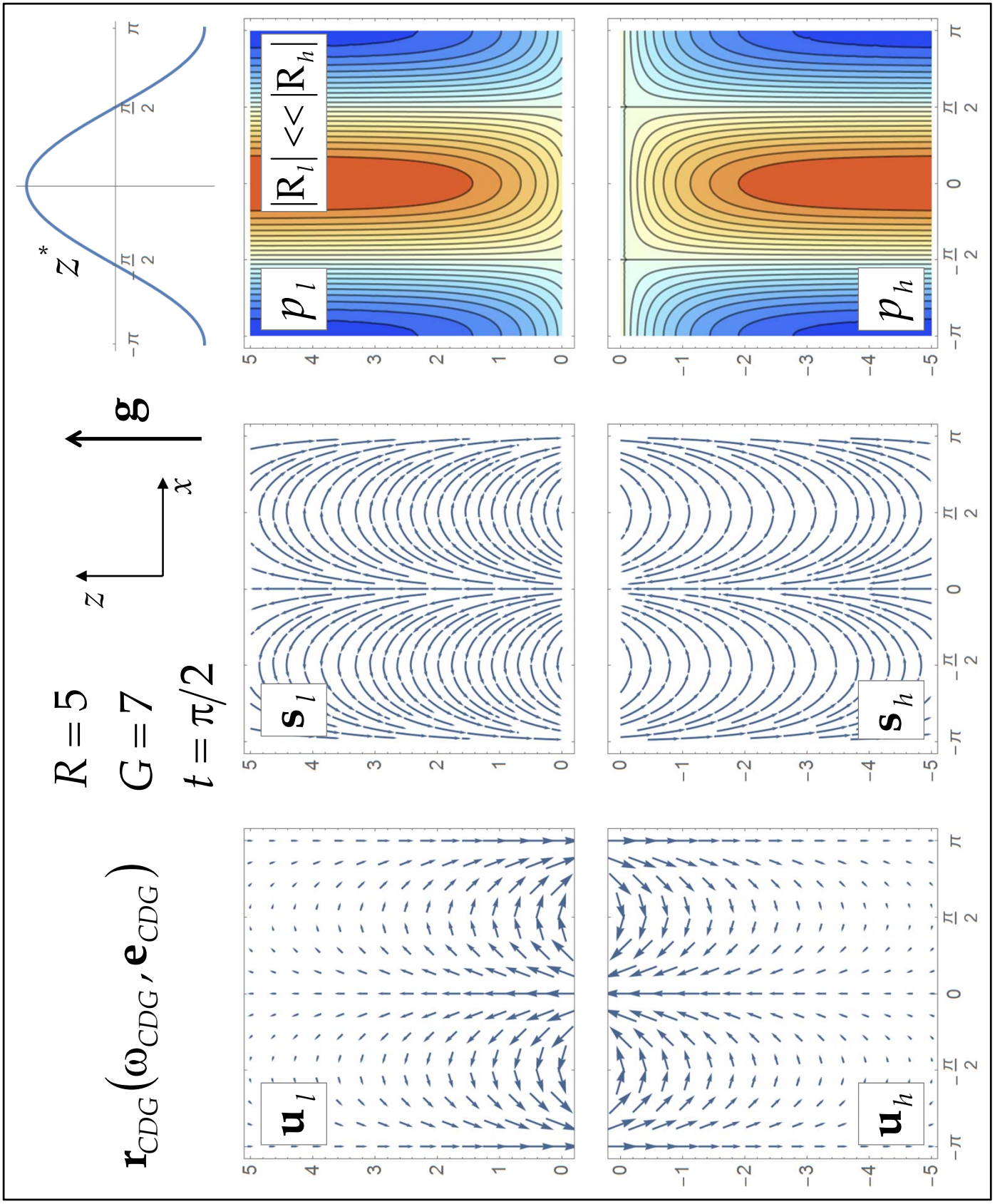
$\mathbf{r}_{CDG}\left(\omega_{CDG}, \mathbf{e}_{CDG}\right)$
$R = 5$
$G = 7$
$t = \pi/2$
z
x
$\mathbf{g}$
z^*
$\mathbf{u}_l$
$\mathbf{s}_l$
p_l
$|\mathrm{R}_l| << |\mathrm{R}_h|$
$\mathbf{u}_h$
$\mathbf{s}_h$
p_h

Fig.6

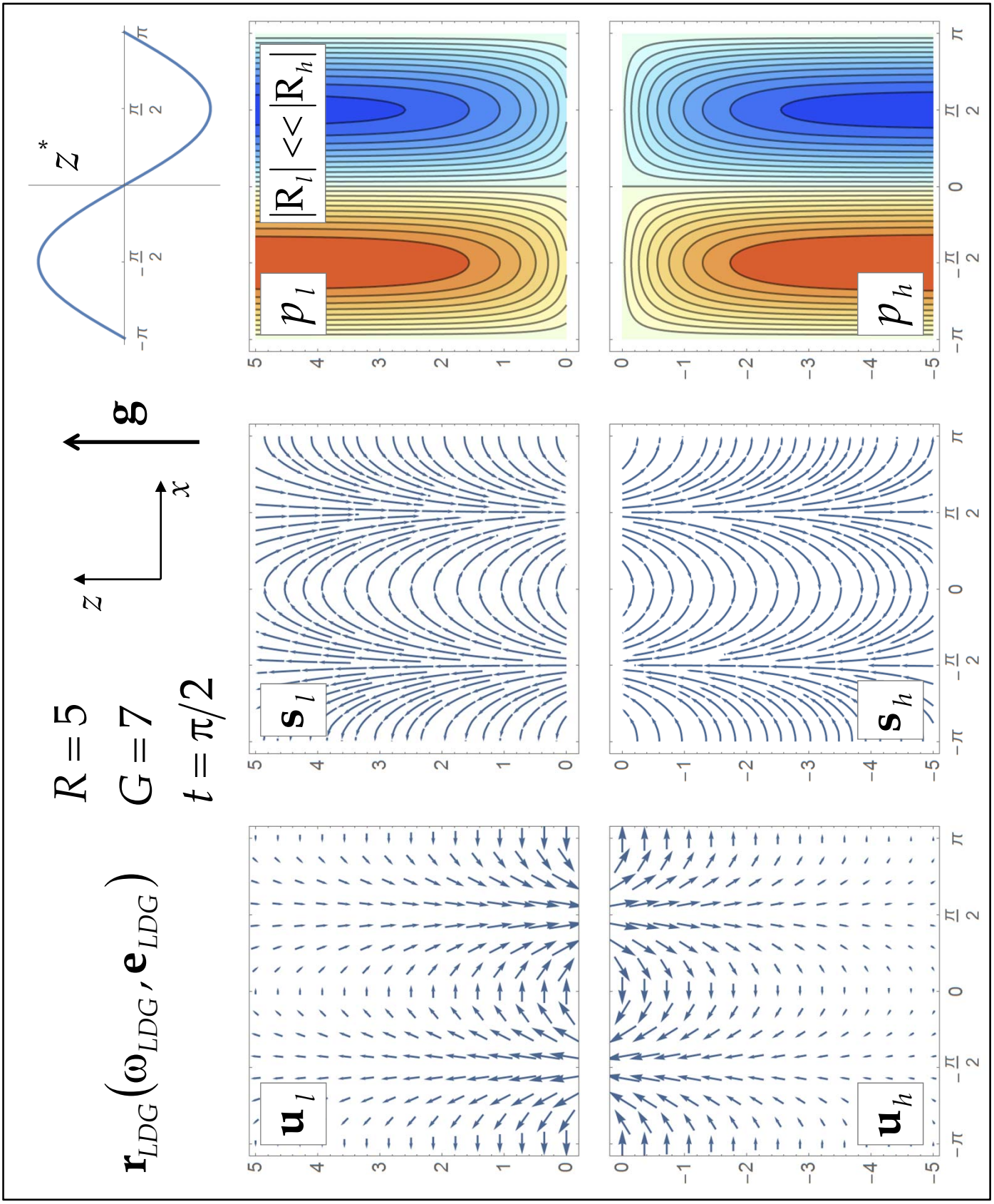
$\mathbf{r}_{LDG}\left(\omega_{LDG}, \mathbf{e}_{LDG}\right)$
$R = 5$
$G = 7$
$t = \pi/2$
z
x
g
z^*
$\mathbf{u}_l$
$\mathbf{s}_l$
p_l
$|\mathrm{R}_l| << |\mathrm{R}_h|$
$\mathbf{u}_h$
$\mathbf{s}_h$
p_h

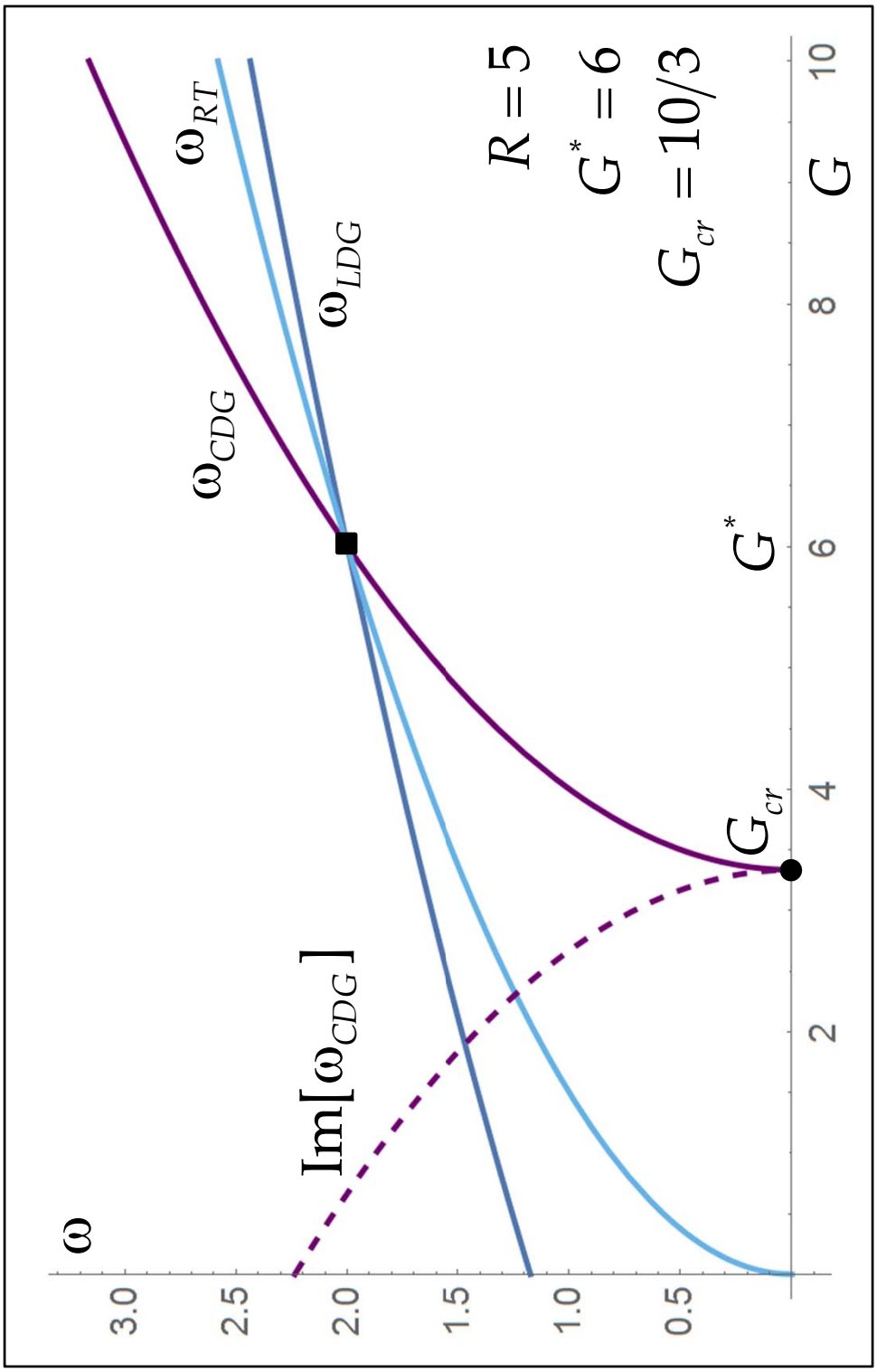
ω
Im[ω_CDG]
ω_RT
ω_LDG
ω_CDG
R = 5
G* = 6
G_cr = 10/3
G_cr
G*
G
3.0
2.5
2.0
1.5
1.0
0.5
2
4
6
8
10

Fig.7